

THE LMC SATELLITES, WHERE ARE THEY? A MODEL OF THE LMC'S FIRST
INFALL

by

IVER B SNEVA

Bachelor of Arts, 2018
University of North Texas
Denton, TX

Submitted to the Graduate Faculty of the
College of Science and Engineering
Texas Christian University
in partial fulfillment of the requirements
for the degree of

Masters of Science

May 2024

THE LMC SATELLITES, WHERE ARE THEY? A MODEL OF THE LMC'S FIRST
INFALL

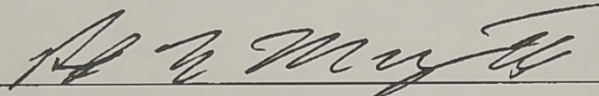
by

Iver B Sneva

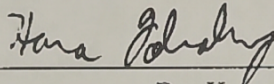
Dissertation Approved:



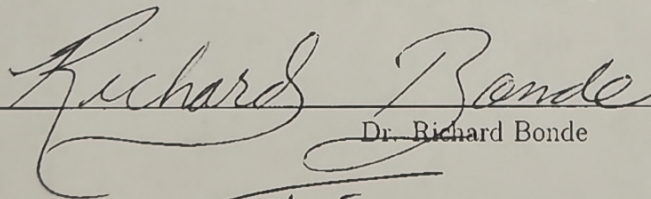
Dr. Mia Bovill



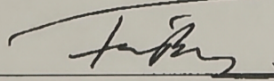
Dr. Peter Frinchaboy



Dr. Hana Dobrovolny



Dr. Richard Bonde



For The College of Science and Engineering

ACKNOWLEDGEMENTS

Dedicated to my late grandfather and role model growing up Captain Terry Schmidt, a hobby astronomer who needed a helper from time to time. Your hobby became my study and for that, with much love, I thank you.

First and foremost, I would like to thank my advisor Dr. Mia Sauda Bovill who's guidance and support has propelled me through my three year journey for my Masters degree at TCU. You took a graduate student who came back to school after a two year hiatus and taught me the value of doing good research, proper coding techniques, teaching pedagogy practices, and being a kind and supportive astronomer. Your understanding of my many unfortunate situations that arose over the course of the past three years allowed me to cope and recover to become stronger than I was. Each year, I became stronger than the last and for that, I cannot thank you enough!

Thank you Dr. Sachi Weerasooriya, my former lab partner and colleague who's help and support through my time in graduate school cannot be understated. I am thankful for all of your insight throughout this process, knowledgeable code troubleshooting, and artistic expertise to help me produce a successful thesis.

Thank you, my department committee: Dr. Peter Frinchaboy, and Dr. Hana Dobrovolny, and Dr. Richard Bonde for taking the time to review this thesis to make it better.

Thank you to my loving parents Lisa and Frank Sherman, my sisters Cristina and Kaylee Sherman, and my grandmother Molly Schmidt. Although we are all in separate states, I have always felt you were there whenever I needed you. Thank you for supporting my many dreams whether that be my pursuits in music or my studies in astronomy, everyone has been a catalyst to my success.

Thank you to my loving dog Buffy who has been a rock of support in my life for over 10 years. She has been through everything with me and got me through the good and bad times. I also want to thank Buffy's second dad and my landlord, roommate, and best friend William DeAlcuaz. Your kindness and generosity has been more than I could possibly ask for and more than I could ever pay back. I am thankful for the two random jam sessions that put us together for it has blossomed into a wonderful long-term friendship.

Special thanks to Dr. Joanna Schmidt for giving me the opportunity of working alongside you during our time at the Koehler Center. Your knowledge and expertise in teaching pedagogy, educational practices, and inclusive learning taught me how to be a better educator. I am thankful for all the fantastic work we did together. Not many people have the opportunity to work with someone and learn from someone as great and kind as you.

Thank you to my best friend Blase Murphy and his family for being my Texas family during my time here. It's thanks to you that Texas has felt as much as home as when

I'm with my family. I've enjoyed getting to be a part of your growing family and look forward to supporting your family the same way you have supported me.

A special thanks to all my many friends who have taken interest and supported my time in graduate school and to me as a person. Your love and support kept the passion in my heart and the drive to see it through. The list of people I could thank is much too long for me to acknowledge every single one of them, but they know who they are.

And finally, thank you to my late grandfather Captain Terry Schmidt. You were my role model growing up who supported me in everything I did. Your inclusion of me with your hobbies helped mold my passions and interests that I have today. Whether it was trains, the American Civil War, or astronomy, you would always find a way to include me in it. You introduced me to astronomy at an early age, observing various stellar objects through your telescope and sparked a lifelong fascination with it. Never would I have guessed I would be doing research in the same field you took a hobby to. Your influence is the reason I am here today and although I miss you dearly, I know you'd be proud. Thank you grandpa and with much love, rest in peace.

Contents

List of Common Acronyms and Terms in Astronomy	viii
1 Introduction	1
1.1 Brief Cosmology	3
1.2 The Local Group	4
1.3 Dwarfs of the LMC	7
2 Simulations and Modeling	11
2.1 Building the Potential	14
2.1.1 The Milky Way	15
2.1.2 The LMC	19
2.1.3 LMC as a Moving Potential	22
2.2 LMC Dwarfs	27
2.2.1 And Around It Goes...	30
2.3 Into the Milky Way	40
3 Observations	43
3.1 Local Group Dwarfs	44
4 Results	52
4.1 Sample Projections	53
4.1.1 100 Run Sample Projections	55
4.1.2 Distance Cutoff of 150 kpc	57
4.2 LMC Mass Dependence	61
4.2.1 100 Run Mass Dependent LMCs	62
4.2.2 Distance Cutoff of 150 kpc for Mass Dependent LMCs	64
5 Conclusion	69
5.1 Conclusion	70
5.2 Looking to the Future	72
5.2.1 N-body Simulations for LMC satellites	72
5.2.2 Curiosities Surrounding M33	72

Vita

Abstract

List of Figures

1.1	Number of dwarf satellites as a function of host mass	6
2.1	Contour plot of the Milky Way potential using the provided potential in Galpy (Bovy 2015)	18
2.2	Contour plot of the Milky Way potential using the provided potential in Galpy (Bovy 2015)	19
2.3	Contour plot of the LMC potential using a Hernquist potential model. . .	21
2.4	6 figure LMC orbital evolution to forward and backward by 6 Gyr	26
2.5	Diagram of our randomized rotation	34
2.6	Histogram showing the initial binding energies of the LMC satellite sample.	35
2.7	LMC satellite sample's positions and velocities.	36
2.8	LMC satellite sample's rotated positions and velocities.	37
2.9	LMC satellite sample's shifted positions and velocities.	38
2.10	6 figure LMC satellite orbital plots	41
3.1	Atoiff projection of all the Milky Way satellites in Galactic coordinates. .	47
3.2	Milky Way satellite distance distribution	51
4.1	Fiducial LMC satellite sample projection for 1 run of it's initial parameters.	53
4.2	Fiducial LMC satellite sample projection for 100 runs.	55
4.3	Fiducial LMC satellite sample 100 run projection < 150 kpc.	57
4.4	Fiducial LMC satellite sample 100 run projection > 150 kpc.	59
4.5	Histogram of the fractional number of satellites from Earth.	60
4.6	Satellite sample projection for 100 runs of less massive LMCs	62
4.7	Different LMC masses satellite sample 100 run projection < 150 kpc. . .	64
4.8	Different LMC masses satellite sample 100 run projection 150 kpc. . . .	65
4.9	Fractal number of satellites from Earth for all LMCs.	67

List of Tables

2.1	LMC Analogs	20
3.1	Known and Suspected LMC Satellites	45
3.2	LMC Satellite candidacy based on the works of Sales et al. (2017) [S17], Kallivayalil et al. (2018) [K18], Erkal & Belokurov (2020) [E/B20], Patel et al. (2020) [P20], and Battaglia et al. (2022) [B22]. Satellite’s candidacy is given by highly likely (+), unlikely (-), uncertain (?), and recently captured/interacting satellites (c). Brackets around the recently captured/interacting satellites are identified as Milky Way satellites that have close encounters with the LMC, but remain satellites of the Milky Way.	46

List of Common Acronyms and Terms

- Star Formation – SF
- Interstellar Medium – ISM
- Semi-Analytical Model – SAM
- Milky Way – MW
- Large Magellanic Cloud – LMC
- Small Magellanic Cloud – SMC
- Ultra Faint Dwarfs – UFD
- Gigayear – Gyr (10^9 years)
- kiloparsecs – 1000 parsecs; 1 parsec (pc)

Chapter 1

Introduction

Dwarf galaxies are the most common type of galaxies in the universe. Their low masses and shallow potential wells make them unique laboratories to study the physics of star formation in a variety of environments. However, even with their high abundance, the star formation physics of dwarf galaxies remains an active area of research to this day.

As with all galaxies, the baryonic evolution of dwarf galaxies is governed by the baryon cycles that regulate star formation. Gas in-falling from the inter-galactic medium (IGM) will flow toward the halo's center. As the gas cools, it will begin to form stars. Star formation (SF) converts interstellar gas into stars, depleting the gas of a given galaxy and feeding back metals, energy, and momentum into the interstellar medium (ISM) via supernova explosions. This feedback from supernova has the ability to expel gas from the galaxy entirely. If a dwarf galaxy is interacting with a more massive galaxy, a large fraction of the expelled gas will be lost to the host halo via tidal and ram pressure stripping.

Though they are the lowest mass galaxies, dwarf galaxies have the largest stellar mass range of any type of galaxy, specifically over six orders of magnitude separates the Large Magellenic Cloud from the ultra-faint dwarfs. The ultra-faint, lowest mass dwarfs have dark matter masses as low as $10^7 M_{\odot}$, at the very least five orders of magnitude smaller than that of our own Milky Way galaxy, and four orders of magnitude less massive than the Large Magellenic Cloud.

With absolute V-band magnitudes as low as $-3 \times L_{\odot}$ and stellar masses as low as a few hundred times that of our Sun, the lowest mass dwarf galaxies are extremely faint. As a result, these ultra-faint dwarf galaxies are most likely to be detected as satellite galaxies

orbiting larger galaxies like our Milky Way. As such, much of our understanding of the star formation physics of these systems is based on the dwarf satellite galaxies of the Milky Way and Andromeda galaxies (Fre 2010). The dwarf satellites of both galaxies show a correlation between various observed properties such as absolute magnitude, surface brightness, half-light radii, metallicities, and stellar velocity dispersion.

Over the last few years, there has been increasing observational and theoretical studies on the dwarf satellites of dwarf galaxies (Kallivayalil et al. 2018, Patel et al. 2020, Erkal & Belokurov 2020). Two Milky Way dwarf satellites that are most likely to host dwarf populations of their own are the Large Magellanic and Small Magellanic Clouds (LMC and SMC respectively).

1.1 Brief Cosmology

Before we discuss the satellites of the dwarf galaxies like the LMC, we need to briefly discuss the cosmology in which they exist. Current best estimates suggest the energy density of the universe is made up of 5% normal baryonic matter, 27% dark matter, and 68% dark energy (Aghanim et al. 2020).

In the modern epoch, dark energy dominates the energy density of the universe with 68% of that total. Effectively nothing is known about its nature, however it is detected via accelerating expansion of the universe during the last eight billion years. Since dark energy only effects the movement of bound systems such as galaxies on 10's to 100's of mega-parsec scales, it has no effect on the evolution of bound structures such as galaxy groups and the dwarf galaxies they contain. Although is an important topic to

understand larger scale cosmology and galaxy evolution, it does not have relevance on the kilo-parsec scales relevant to this work, however we have included a brief description of it for completeness.

Dark matter makes up 27% of the total energy density of the universe and more than 80% of the matter in the Universe (Aghanim et al. 2020). It does not emit or absorb light and therefore can only be detected by the gravity it exerts. While there are more constraints on its nature than dark energy, we do not know what dark matter is. All galaxies exist in dark matter halos, whose mass determines the depth and shape of the gravitational potential well of the galaxy. The evidence for dark matter comes from the effect of gravity on the visible baryonic matter. The measured potential wells of galaxies via kinematics of the stars (Rubin & Ford 1970) and bending of light by gravitational lensing (Hoekstra et al. 2013) cannot be explained by the visible baryonic matter alone. In this work, the gravitational potentials are dominated by the assumed dark matter halos in which the Milky Way and the LMC are assumed to reside.

1.2 The Local Group

We now move from a more general discussion of dwarf galaxies and cosmology into the specifics of the galaxy group in which the Milky Way and LMC reside, aptly named the Local Group (LG). The Local Group comprises two massive galaxies, the Milky Way with a mass of $0.8 - 1.8 \times 10^{12} M_{\odot}$ (Kallivayalil et al. 2018, Battaglia et al. 2022, Sales et al. 2017) and Andromeda, or M31, with a mass of $\sim 12.3_{-6}^{+18} \times 10^{11} M_{\odot}$ (Evans & Wilkinson 2000), a smaller galaxy M33, and their dwarf satellite systems.

The most luminous and massive of the Milky Way’s dwarf satellites is the LMC. The LMC mass ranges from $0.2 - 3.0 \times 10^{11} M_{\odot}$ (Battaglia et al. 2022, Erkal & Belokurov 2020, Kallivayalil et al. 2018, Patel et al. 2020) with a stellar mass ($\sim 3 \times 10^9 M_{\odot}$) and a gas mass ($\sim 5 \times 10^8 M_{\odot}$) (Vasiliev 2023). The second most massive dwarf satellite of the Milky Way, the SMC, is part of the same system as the LMC. The LMC has a greater mass in comparison to the SMC, with a mass-ratio of $\sim 10 : 1$ (Besla et al. 2007), meaning the dark matter mass of the SMC is about 1% of the Milky Way’s.

Importantly, the Magellanic Clouds are on their first infall into the Milky Way (Besla et al. 2007) and gas from the LMC/SMC has formed the Magellanic Stream. In addition, there also exists a leading tidal arm that is interacting with the Milky Way disk upon first infall (Barger et al. 2019).

The LMC is massive enough that it should have a significant number of satellites of its own (Bovill & Ricotti 2011), however before 2017, we had never seen a confirmed LMC satellite. With GAIA DR2, all that changed. The second GAIA data release (DR2) found over 30 new ultra-faint dwarf (UFD) satellites close to the Magellanic Clouds (Patel et al. 2020, Kallivayalil et al. 2018). The Proper Motions (PMs) of these satellites were determined from the GAIA DR2 and studies of Magellanic candidacy began. The DR3 release of GAIA has furthered the search for Magellanic candidacy, providing more potential candidates to be studied (Battaglia et al. 2022). As seen in Figure 1.1, the most massive dwarf galaxies will have satellite galaxies of their own with the number of satellites decreasing with the mass of host. As such, the vast majority of dwarf satellites that originated with the LMC/SMC system would have originally belonged to the LMC.

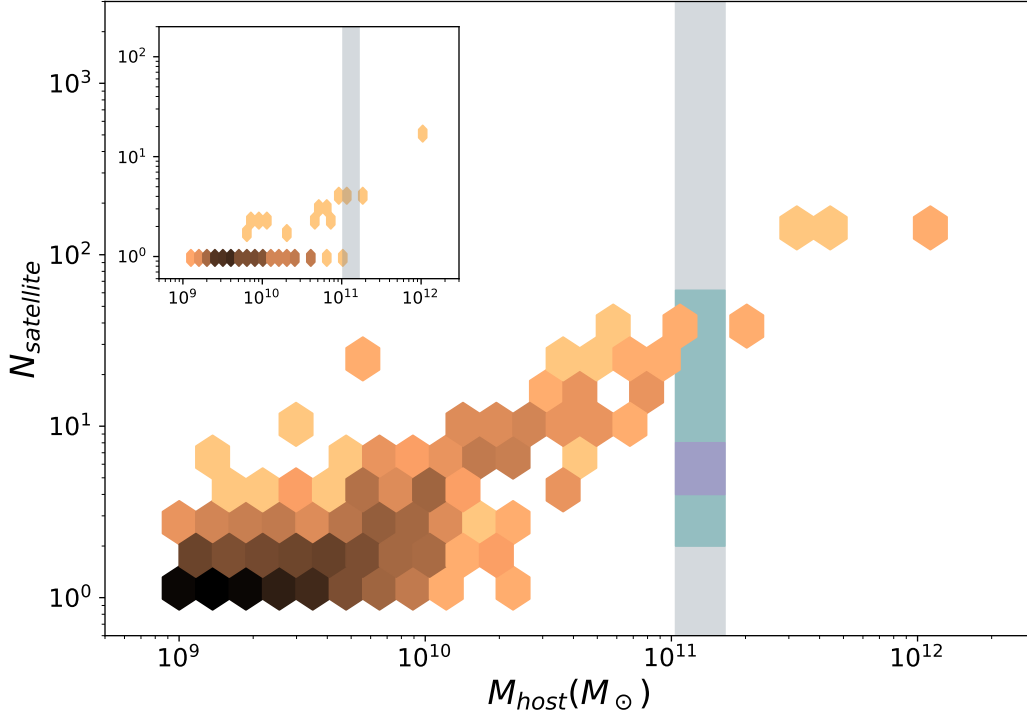


Figure 1.1: Number of luminous satellites as a function of host halo mass. We define a luminous satellite as a subhalo that is either a non-fossil or contains a primordial stellar population. The grey shaded region shows the mass range for the LMC (Erkal 2019) and the teal bar is the estimate of observed Milky Way satellites associated with the LMC from Deason et al. (2015). The purple bar show the number of known satellites associated with the LMC (Pardy et al. 2020). This is an updated version of Figure 5 from Bovill & Ricotti (2011).

Based on observations, the number of dwarf satellites around the LMC was estimated to be small, somewhere between $\sim 5 - 10$ UFDs (Patel et al. 2020). However, this number is at least a factor of two below the number of faint dwarf satellites predicted for a dark matter halo of the LMC’s mass (Bovill & Ricotti 2011). This discrepancy sets up the primary question of this thesis of finding where the “missing” LMC satellites are.

1.3 Dwarfs of the LMC

Before we can go looking for the “missing” dwarfs, we need to talk a bit more about the ones we have found. Satellites of the Magellanic Cloud are composed of UFD satellites and classical dwarf spheroidal satellites (Patel et al. 2020). There is a correlation between the number of satellites and the masses of the Milky Way galaxy and the LMC (Patel et al. 2020, Bovill & Ricotti 2011). To determine if a satellite came in with the LMC, satellites have their 3-D positions and 3-D velocities tested (Erkal & Belokurov 2020). Proper Motions of dwarf satellites can be pulled from the GAIA DR2 and GAIA DR3 (Erkal & Belokurov 2020, Kallivayalil et al. 2018, Battaglia et al. 2022, Patel et al. 2020) with criteria being set to choose specific satellites.

With the release of GAIA DR2 came an in-depth look into dwarf galaxies. GAIA DR2 featured enhancements to get better, more accurate measurements of positions and Proper Motions. They had two different methods in the G-band to find positions with five-parameter and two-parameter astrometry. Proper Motions were determined using the five-parameter astrometry. For brighter G-bands objects ($G < 15$) low uncertainties were given (0.02 - 0.04 mas) for positions and parallax in the five-parameter astrometry. Fainter objects ($G = 21$) had a higher uncertainty (2 mas) in the five-parameter astrometry. For the two-parameter astrometry, there was much higher uncertainty (1 - 4 mas) for position compared to the five-parameter astrometry. Proper Motions follow a similar convention to the position and parallax of the five-parameter astrometry. The Proper Motion of brighter objects ($G < 15$) has a lower uncertainty (0.07 mas yr^{-1}) than the uncertainty of fainter objects (3 mas yr^{-1} at $G = 21$). Proper Motion could only be

found in the five-parameter astrometry. They note a low systematic astrometric error (average over the sky) to be < 0.1 mas (Gaia Collaboration et al. 2018).

With Proper Motions being pulled from GAIA DR2, satellites can be determined if they have relation to the LMC. GAIA DR2 allows for the measurement of Proper Motions of the lowest-mass, UFD galaxies in the Milky Way halo (Patel et al. 2020). Using GAIA DR2, 32 low mass dwarf galaxies were considered LMC satellite candidates due to their proximity to the LMC with 50% of candidates having a $> 70\%$ association with being Magellanic Cloud satellites (Kallivayalil et al. 2018). With the LMC close to pericenter, much debris north of the LMC in the northern hemisphere is further out and moving away from the LMC which ruled out many of the potential LMC satellites. However, there are many more potential LMC satellites in the southern hemisphere. Although debris may be further out, it is moving in and has not yet reached pericenter (Sales et al. 2017). Next, we talk about these low mass dwarf galaxies and which of them are considered satellites of the LMC.

Low mass dwarfs, called Ultra Faint Dwarfs, are a sub-classification of classical dwarf galaxies ($10^5 - 10^7 M_\odot$) and are defined by having luminosities that are $L \leq 10^5 L_\odot$ and masses of $10^2 - 10^5 M_\odot$ (Richstein et al. 2024). UFD galaxies have low luminosities ($M_V > -8$) that correlate to smaller stellar masses ($M_* < 10^4 M_\odot$) (Sacchi et al. 2021). LMC candidacy research has been explored using a variety of techniques across different works for UFDs. Carina 2, Carina 3, Horologium 1, and Hydrus 1 have radial velocity measurements from the GAIA DR2 compared to 3-D kinematics of UFDs to the LMC debris (Sacchi et al. 2021, Patel et al. 2020). Color-Magnitude Diagram (CMD) work from Battaglia et al. (2022) confirmed that Carina 2, Carina 3, and Hydrus 1 are

LMC satellites. Seven systems of dwarfs have been found whose positions make them likely LMC candidate: Horologium 1, Horologium 2, Eridanus 3, Reticulum 3, Tucana 5, Tucana 4, and Phoenix 2 (Sales et al. 2017). Patel et al. (2020) confirms Reticulum 2 is considered a Magellanic satellite that was recently captured. Working with GAIA DR3, Battaglia et al. (2022) found that the satellites Carina 2, Carina 3, Horologium 1, Hydrus 1, and Phoenix 2 are long-term Magellanic satellites. Work by Kallivayalil et al. (2018) shows that Hydra 2 and Draco 2 have possible association with the LMC. Some satellites like Tucana 4 and Grus 2 are recently captured satellites by the LMC in the last ~ 500 Myrs. However, Tucana 4 is believed to have origins to (be parented by) the LMC system whose orbit may have been highly perturbed by the SMC. Grus 2 did not originate within the Magellanic system, believed to be captured in the last 200 Myr (Battaglia et al. 2022).

While we have found (8) known and (6) suspected dwarfs of the LMC, it is still below the predicted number in (Bovill & Ricotti 2011). Early predictions of the number of LMC satellites predicted the number of satellites to be 70^{+30}_{-40} . Improved information with the proper motions (PMs) of satellites helped to refine the predicted satellites down to ~ 60 (Erkal & Belokurov 2020)). With the mass of the LMC being only an order of magnitude smaller than that of the Milky Way, dynamical effects are present when interacting with one another. However, this would mean that the Milky Way should be stripping away LMC satellites and taking them as their own (Vasiliev 2023). Even with a long list of known and potential LMC UFDs, it does not fully account for all the satellites theoretically thought to be there (Bovill & Ricotti 2011). There should be more UFDs that originally belonged to the LMC but we do not see them.

This thesis will begin to answer that question. In Chapter 2 we describe the methodology used to model the dynamics evolution of LMC satellites in the potential of the Milky Way-LMC system. In Chapter 3, we provide a more detailed summary of the observations, including the selection of the sample of known and suspected LMC dwarfs. Our results, including a comparison to observations, are presented in Chapter 4 and we present our conclusions and future work in Chapter 5.

Chapter 2

Simulations and Modeling

In this chapter, we describe how we set up our model for our Milky Way/LMC system. We will discuss how we build our simulated Milky Way and LMC systems to test the satellites in orbit around the LMC.

Our model will look at the infall of the LMC with its satellites into the Milky Way for the first time. We want to see what effects the Milky Way has upon first infall of the LMC and the satellites orbiting it. Many unknowns exist in the LMC system and we must find a way to account for some of these. These unknowns include the mass of the LMC, excluding the SMC from our model, and the orbit/orientation of satellites around the LMC. In this chapter, we will discuss how we built a reliable model that accounts for these unknowns.

The mass of the LMC is still uncertain. A range of LMC mass have been tested in various studies. The works of Patel et al. (2020) use three LMC masses of $0.8 \times 10^{11} M_{\odot}$, $1.8 \times 10^{11} M_{\odot}$, and $2.5 \times 10^{11} M_{\odot}$. Erkal & Belokurov (2020) used a range of different LMC masses from $0.2 \times 10^{11} M_{\odot}$ to $3.0 \times 10^{11} M_{\odot}$ in their work. Other works from Battaglia et al. (2022), Kallivayalil et al. (2018) also used LMC masses within these ranges. The consensus today is an LMC mass of $\sim 1.38 \times 10^{11} M_{\odot}$ (Erkal et al. 2019). The LMC has a companion galaxy called the SMC. However, in our models, the SMC is omitted when building our potentials. With a LMC:SMC mass ratio of $\sim 10 : 1$, the SMC does not significantly affect the orbital history of the LMC (Besla et al. 2007) and its exclusion does not significantly affect the total number of Magellanic satellites (Patel et al. 2020). Some works have included an SMC potential in conjunction with an LMC and MW potential like in Patel et al. (2020). However, with the SMC potential having a mass of 1 - 2 orders of magnitude smaller than that of the LMC potential, its

impact on galaxies associated with the LMC was negligible. With the many uncertainties of the LMC and the negligible impact the SMC had on previous works, we make the assumption that the effects of an SMC on our results would be negligible and would introduce significant complications in the mass and orbits relative to the LMC upon infall. We also do not know orbits of the satellites around the LMC before first infall.

We need a method to properly tackle all these unknowns. We must first start by building the static potentials of the Milky Way and LMC. Once our potentials are built, we can move the LMC potential into the static Milky Way potential on the known LMC orbit and place satellites in orbit around the LMC as it moves. We are fortunate that a realistic Milky Way potential used for modeling exists in a python package called `Galpy` (Bovy 2015). `Galpy` does not have a set model for an LMC potential, however, it provides us with the tools to build one for ourselves. We can build our LMC potential using a Hernquist potential profile. This will give us our static LMC potential. Once we have our static Milky Way and LMC potential models built, we then need to make it a moving potential as it is on first infall with the Milky Way.

Moving the LMC forward has it's challenges as we do not know the LMC's initial positions or velocities. We solve this by using the orbital integration function in `Galpy` to rewind the LMC back in time. This will give us our initial parameters necessary to move the LMC forward into the Milky Way. Details on this will be explained later in the chapter.

Once we have our potentials built and can move them, we need to place satellites in orbit around the LMC potential as we move it forward. We will treat the LMC satellites as test particles around the LMC potential. Once we have our LMC and it's

satellites initial 6-D parameters, we can evolve forward the LMC and its satellites as it goes through first infall. All of these processes will be discussed in greater detail in later sections. Let's start by looking how we built each of our potentials for our models.

2.1 Building the Potential

Our first step is to build our Milky Way and LMC gravitational potentials. Gravitational potentials are based on the distribution of mass of a galaxy. These potentials determine the gravitational force felt by any objects interacting with the galaxy. Each galaxy has a certain gravitational force associated with it. This can be calculated based on the mass of the two objects interacting with each other by the gravitational constant, divided by the distance between the two objects squared. Given by the following equation

$$U = - \int_{r_0}^r \vec{F} \cdot d\vec{r}, \quad (2.1)$$

where F represents the gravitational force of two objects interacting with each other given as

$$F = -\frac{GMm}{r^2}. \quad (2.2)$$

We are making the assumption that both the LMC and MW are time-invariant or static potentials. This assumption is made because neither potential has gone under a major merger event in the time frame of 6 Gyr. Details of our time frame will be explained further in section 2.1.3. In the case of the LMC, since we do not know anything about

it's merger history, it is unknown if it has gone under any sort of merger history and thus we elect to keep it as a static potential.

The first potential we build will be our Milky Way potential. As discussed in the previous section, we have a realistic Milky Way potential we can use for our model. Next, we will build an LMC potential as a static Hernquist potential to describe the dark-matter halo of the LMC. We will orbit our LMC potential around the Milky Way over a time frame of 6 Gyr. Once we have these two potentials built, we can stick in our LMC satellites as test particles orbiting around the LMC as it moves toward it's first infall with the Milky Way. This will allow us to model our satellites around the LMC as it orbits the Milky Way. Before we discuss modeling the LMC satellites, we must discuss in greater detail the Milky Way and the LMC potentials.

2.1.1 The Milky Way

As previously stated, we will start by building the Milky Way potential as this is both the most massive galaxy in our system and can be easily built. Galpy offers a simple, easy to use model of the Milky Way potential we can use (`MWPotential2014`) for our model (Bovy 2015). The `MWPotential2014` was developed to fit a larger range of dynamical data for the Milky Way and allows for use of a realistic Milky Way potential and is a combination of three potentials (see Figure 2.1), a Hernquist bulge model, a Miyamoto Nagai potential disk, and a dark-matter halo modeled as a Navarro-Frenk-White (NFW) potential (Bovy 2015). The bulge and dark-matter halo models were calculated using

similar calculations for density, potential, and the R and Z components of the force and are given as:

$$\rho(R, Z) = \rho_d e^{\frac{R}{R_d} \frac{|Z|}{z_d}} \quad (2.3)$$

$$\Phi(R, Z) = -4\pi G \rho_d \int_0^\infty dk J_0(kR) \left(k^2 + \frac{1}{R_d^2}\right)^{-\frac{3}{2}} * \frac{e^{-k|z|} - kz_z e^{\frac{-|z|}{z_h}}}{(1 - kz_h)^2} \quad (2.4)$$

$$F_R(R, Z) = -4\pi G \rho_d \frac{z_h}{R_d} \int_0^\infty dk k J_1(kR) \left(k^2 + \frac{1}{R_d^2}\right)^{-\frac{3}{2}} * \frac{e^{-k|z|} - kz_z e^{\frac{-|z|}{z_h}}}{(1 - kz_h)^2} \quad (2.5)$$

$$F_Z(R, Z) = (\text{sign}(z)) 4\pi G \rho_d \frac{z_h}{R_d} \int_0^\infty dk k J_0(kR) \left(k^2 + \frac{1}{R_d^2}\right)^{-\frac{3}{2}} * \frac{e^{-k|z|} - kz_z e^{\frac{-|z|}{z_h}}}{(1 - kz_h)^2}, \quad (2.6)$$

where $J_i(\cdot)$ is a strongly oscillating Bessel function integrated between each zero to k of the function. Our k parameter is dependent on the initial and final radial length (R and R_0 respectively). The remaining parameters in the equations above are the Z component (height above or below the disk), the R_d component (scale lengths), and the z_d component (scale height of the stellar exponential disk component). Further explanation is explored within Bovy & Rix (2013) and points to other works for justification of the process. As stated in the previous section, we are treating our Milky Way as a static potential because of the lack of a major merger in the time frame of the past 6 Gyr. Material may have been accreted during this time frame, however, this has not significantly changed our potential.

The mass of `MWPotential2014` is provided in Bovy (2015) ($M_{MW} = 0.8 \times 10^{12} M_\odot$). A similar Milky Way potential was developed with the same mass to find probabilities of potential LMC satellites (Erkal & Belokurov 2020). In Fig 2.2, we show the contour

plot of our Milky Way potential as a function of R/R_0 versus z/R_0 where R is the radial distance of the Milky Way, z is the height above/below the Milky Way disk, and R_0 the distance to the Galactic center fixed to a distance of 8 kpc (Bovy 2015).

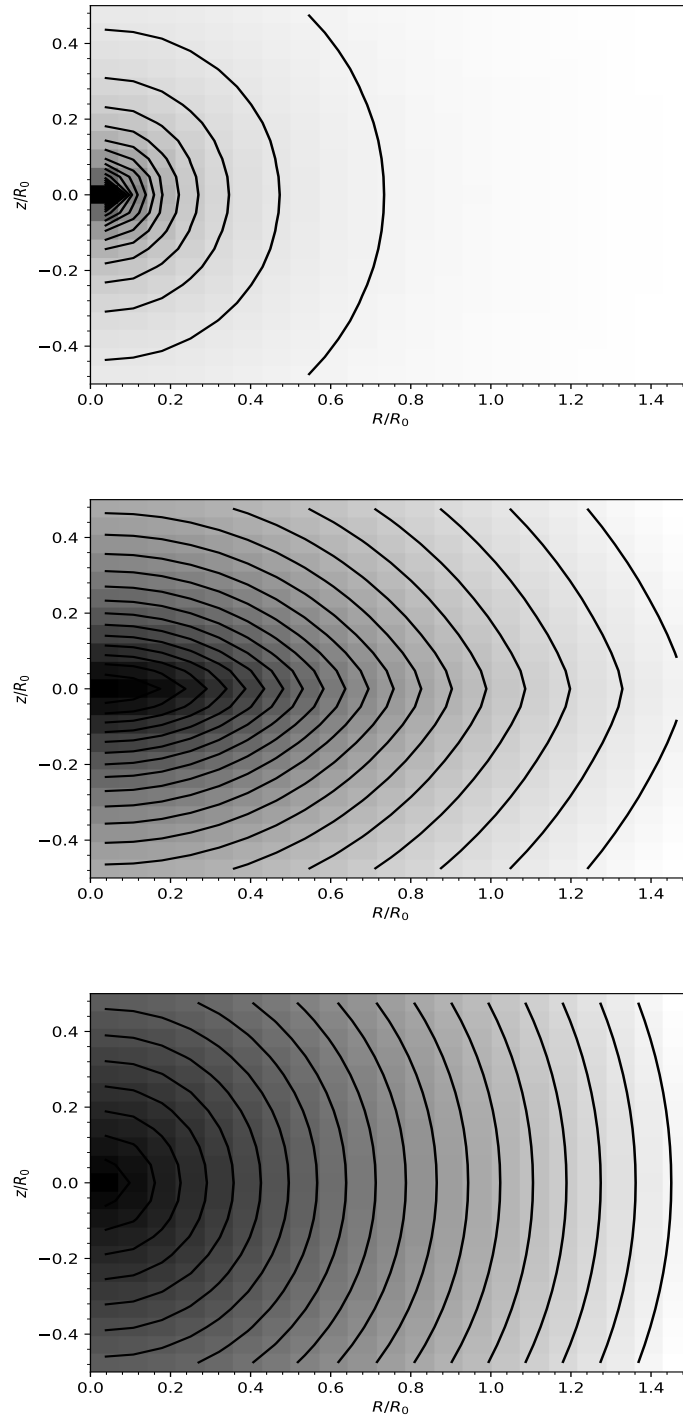


Figure 2.1: Contour plots of each potential component of `MWPotential2014` from Galpy Bovy (2015). The bulge of the Milky Way disk is modeled by a Hernquist potential (top). The disk of the Milky way is modeled by a Miyamoto Nagai potential (middle). The dark-matter halo is modeled by a NFW potential. R represents the radial distance of the each potential, z represents height above/below the disk for each potential, and R_0 the distance to the Galactic center (set at 8 kpc). The contours are linearly spaced. These potentials are combined to model Galpy's `MWPotential2014` (see Figure 2.2)

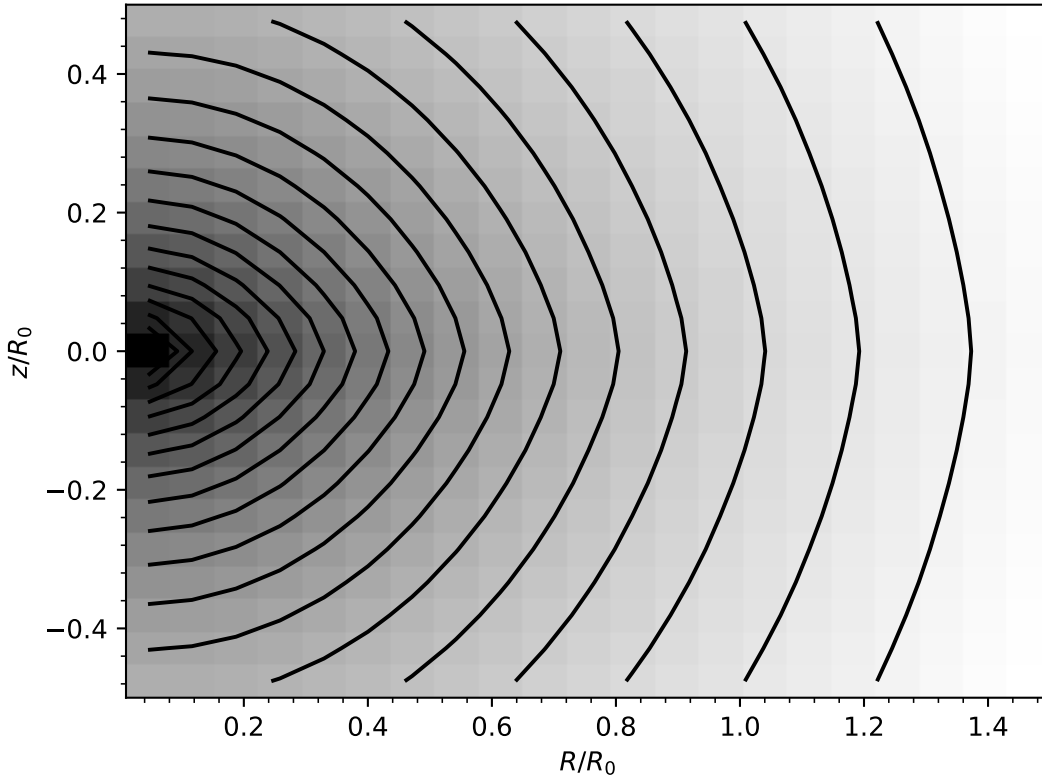


Figure 2.2: Contour plot of the Milky Way potential using the `MWPotential2014` from Galpy Bovy (2015). R represents the radial distance of the Milky Way, z represents height above/below the disk, and R_0 the distance to the Galactic center (set at 8 kpc). The contours are linearly spaced.

2.1.2 The LMC

Our next step is to set up a static LMC potential. This is less straightforward than for the Milky Way potential since the LMC comes with a few unknowns. We will start by giving a mass to the LMC. The mass of the LMC is uncertain, but narrowed down to what it potentially should be. Many works have used a large mass range of the LMC from $0.2 \times 10^{11} M_\odot$ to $3.0 \times 10^{11} M_\odot$. A massive LMC is up to $M_{LMC} = 3.5 \times 10^{11} M_\odot$ (Erkal & Belokurov 2020). With our model, we have access to this range of LMC masses

and choose our fiducial model to be $M_{LMC} = 1.32 \times 10^{11} M_{\odot}$, close to the present day accepted mass of the LMC. We also will use a range of LMC masses to test our results. Our LMC masses listed in Table 2.1 are the masses discussed later in this chapter. Note that our LMCc is our fiducial mass.

Table 2.1: LMC Analogs

Analog	Mass (M_{\odot})
LMCa	$0.52 \times 10^{11} M_{\odot}$
LMCb	$0.91 \times 10^{11} M_{\odot}$
LMCc	$1.32 \times 10^{11} M_{\odot}$
LMCd	$2.20 \times 10^{11} M_{\odot}$
LMCe	$3.27 \times 10^{11} M_{\odot}$

With the mass of our LMC potential determined, we must now create the potential of the LMC. There are two methods for setting an LMC potential, using either a Hernquist or NFW Profile potential model. We choose to use a Hernquist potential model to set up our static LMC potential. Hernquist potential LMC models have been used in previous works (Patel et al. 2020, Erkal & Belokurov 2020). The reasoning for using Hernquist potential over an NFW Profile potential is the parameters required to create it. The Hernquist potential requires two parameters to make the potential, the mass and a scaled radius of the LMC. The NFW Profile potential required had an additional concentration parameter that we do not have in our models. Our models test over a range of LMC masses similar to that of Erkal & Belokurov (2020) who also used a single Hernquist profile to test LMC satellite probabilities. The Hernquist potential can be calculated in the following way using Galpy

$$\rho = \frac{A}{4\pi a^3} \frac{1}{\left(\frac{r}{a}\right)\left(\frac{1+r}{a}\right)^3}, \quad (2.7)$$

where A is the amplitude of the applied potential using the mass of our LMC, a is the scale radius of our LMC selected, and r is the Galactocentric radial component (Bovy 2015). In Fig 2.3 we show the contour plot of our LMC as a Hernquist potential as a function of R/R_0 versus z/R_0 . The parameters R and z are the same as for the Milky Way potential but use the LMC R and z values.

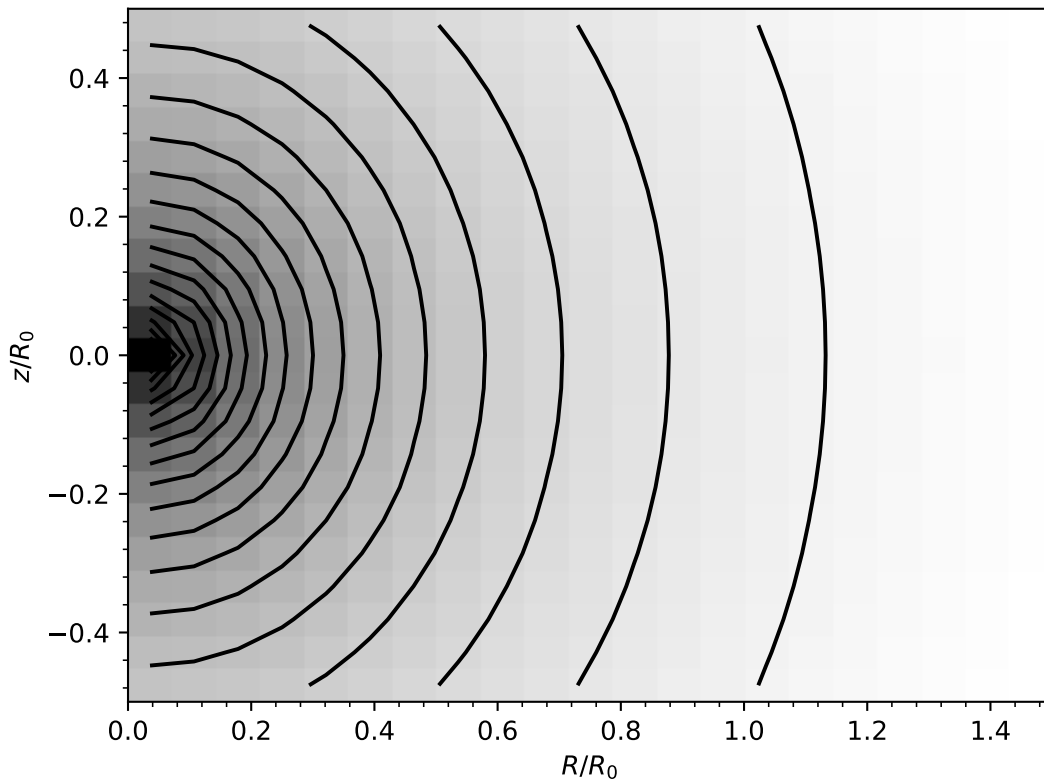


Figure 2.3: Contour plot of the LMC potential using a Hernquist potential profile. Parameters are the same as above, but describe R and z for their respective LMC values.

2.1.3 LMC as a Moving Potential

Now that we have two static potentials built, we need to move our potentials. We can set it up our LMC potential to move on an orbit that will put it on first infall of the Milky Way. To do this, we use the `MovingObjectPotential` function of Galpy (Bovy 2015). We are going to discuss in further detail how we set up our moving potential for our model.

Galpy can simulate a moving potential using the `MovingObjectPotential` function by adding up all potentials in a system with an integrated Galpy orbit (Bovy 2015). Orbital integration for our model is done in a 3-D cylindrical coordinate system and requires the radial distance (R), the radial velocity (v_R), the tangential velocity (v_T), the height with respect to the plane (z), the velocity above/below the plane (v_z), and the azimuthal angle (ϕ) Bovy (2015). We treat the LMC as a moving potential, allowing us to evolve positions and velocities in time as the center of the LMC falls into the Milky Way, modeling first infall. Since we are dealing with two galaxies with different masses, we must also account for dynamical friction between our two potentials. Next, we will talk about how and why we included dynamical friction in our moving potential.

Since the mass of the Milky Way is large compared to the LMC, orbits of smaller satellite galaxies like the LMC will be subjected to some dynamical friction. Dynamical friction (df) is a frictional force of gravitational origin that occurs when a massive object travels through low-mass objects. In our case, this will be our LMC potential through the Milky Way potential.

Galpy has a package that can add dynamical friction to a potential and uses the Chandrasekhar dynamical friction force equation (Bovy 2015)

$$F(\mathbf{x}, \mathbf{v}) = -2\pi[GM][G\rho(\mathbf{x})]\ln[1 + \Lambda^2][\text{erf}(X) - \frac{2X}{\sqrt{\pi}}\exp(-X^2)]\frac{\mathbf{v}}{|\mathbf{v}|^3}, \quad (2.8)$$

where G is the gravitational constant, M is the satellite galaxy mass, \mathbf{x} and \mathbf{v} are the position and moving velocity of that satellite galaxy through a background density ρ . X is calculated as $X = \frac{|\mathbf{v}|}{\sqrt{2}\sigma_r(r)}$. The factor of Λ goes into a Coulomb logarithm, taken as the following equation

$$\Lambda = \frac{r/\gamma}{\max(r_{hm}GM/|\mathbf{v}|^2)}, \quad (2.9)$$

where γ is a constant and should be an absolute value of the density $\gamma = \frac{d\ln(\rho)}{d\ln(r)}$ (Bovy 2015).

The Chandrasekhar Dynamical Friction Force is dependent on the velocity dispersion of the halo and can be calculated, if not explicitly given, from the spherical Jeans equation (Bovy 2015). Adding velocity dispersion is an extra feature allowed in Galpy, however it is not necessary in order to compute the Chandrasekhar Dynamical Friction Force. It can be computed using the LMC's mass and the density of our `MWPotential2014` potential to give us our dynamical friction force.

We use the mass chosen for our LMC, a half-mass radius of 5 kpc as done in the Galpy orbital documentation, and the density of the Milky Way potential to get the dynamical friction. The half-mass radius of 5 kpc will encompass any LMC mass we decide to investigate in our model with negligible effects on the results (Bovy 2015).

This dynamical force can be added to our moving potential as an additional parameter for the LMC's orbital evolution of our model.

With our static LMC set up as a Hernquist model, we can evolve it back in time by 6 Gyr to find its initial 6-D parameters. We have the present day parameters for the LMC from the works of Besla et al. (2007). However, where it initially was before its first infall into the Milky Way remains a mystery. Solving where the LMC was before first infall is our next task. To do this, we can evolve the orbit of the LMC backwards 6 Gyr in time from its present day parameters to find where the LMC was before first infall. This can be confirmed by running our found initial parameters forward to the present day to return it to its original values. Motivation to rewinding the LMC back 6 Gyr is done in the works Erkal & Belokurov (2020) where they rewind the LMC back by 5 Gyr. Further supported that a satellite's probability of being associated with the LMC is not sensitive to a choice of time integration. Rewind times of 3 and 7 Gyr changed the probabilities of satellites being bound to the LMC by $\sim 3\%$. Additionally, a 6 Gyr rewind has shown to match well with orbits of satellite galaxies where earlier time frames deviate in their results. There is also a correspondence of MW-mass galaxies acquiring $\sim 80\%$ of their mass by 6 Gyr. Finally, it takes satellites between $\sim 5-7$ Gyr to complete multiple orbits around the Magellanic Clouds (Patel et al. 2020). Integration times of 6 Gyr allows us to test different masses of the LMC and achieve results for their dwarf satellites. Using Galpy, we can find the time of first infall of the LMC first by running the LMC orbit backwards to 6 Gyr and confirmed this by running the simulation forward from 6 Gyr to present.

In Fig 2.4, we can see our process for rewinding the LMC's orbit back in time by 6 Gyr. We plot the time frame of 6 Gyr versus the six parameters needed for the orbital integration (R_{GC} , z_{GC} , ϕ , v_R , v_T , and v_z). The light blue dashed line represents the LMC orbit the evolution back 6 Gyr. The dark blue dashed line represents the LMC orbit from it's position back 6 Gyr forward to present day.

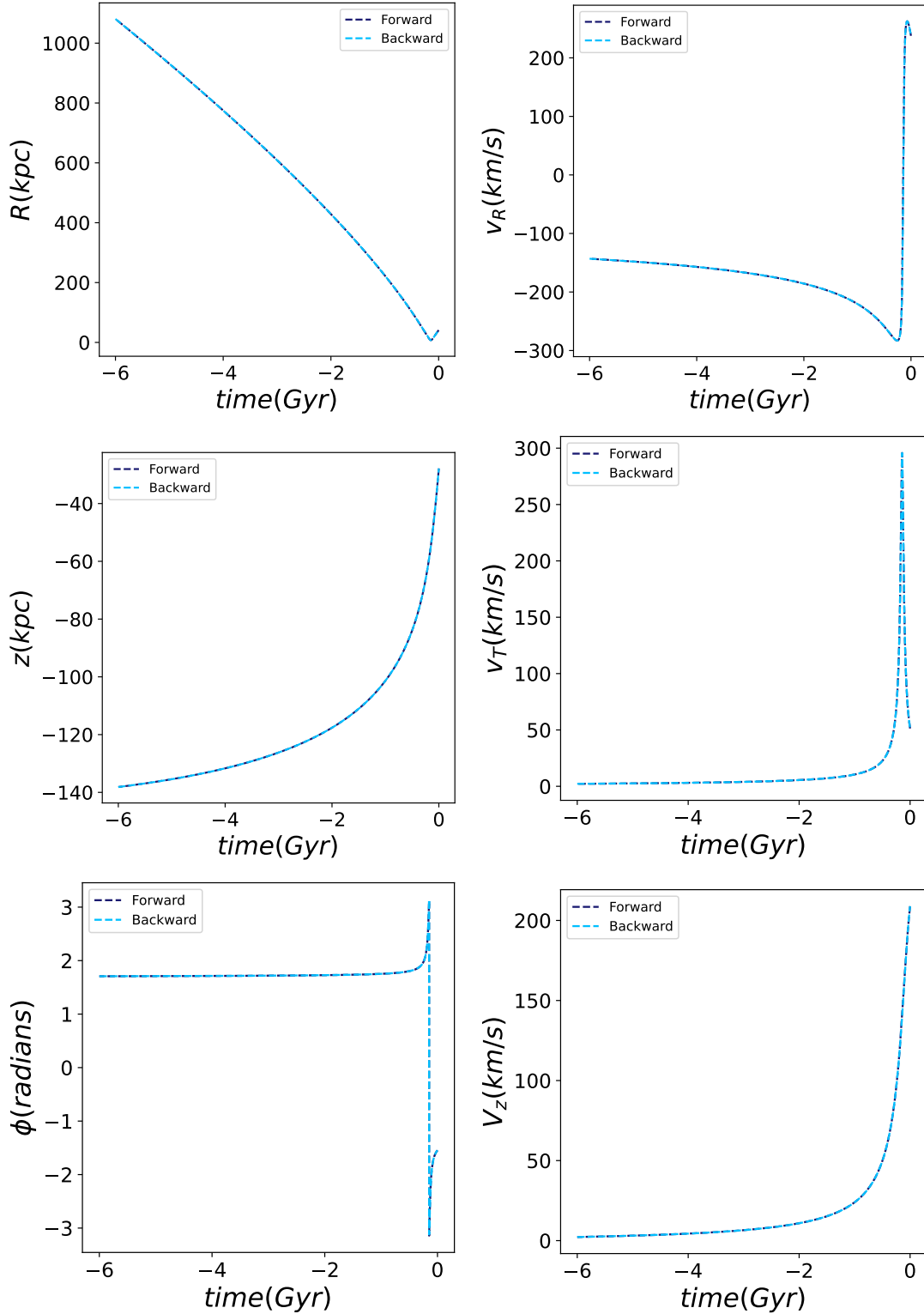


Figure 2.4: The figure above shows the evolution of the LMC's orbit back 6 Gyr (light blue dashed line) and the evolution forward by 6 Gyr (dark blue dashed line) to first infall. Our six plots show time (Gyr) versus the six parameters of the LMC's orbit, $R_{GC}(kpc)$ (top left), $z_{GC}(kpc)$ (middle left), $\phi(Radians)$ (bottom left), $v_R(km/s)$ (top right), $v_T(km/s)$ (middle right), and $v_z(km/s)$ (bottom right).

An assumption we make is keeping the LMC mass constant during our time frame of 6 Gyr. Given the uncertainties surrounding the LMC, this will help not to over complicate our model. Models that built their own LMC potentials use multiple fixed masses to test their theories (Battaglia et al. 2022, Erkal & Belokurov 2020, Patel et al. 2020, Kallivayalil et al. 2018, Sales et al. 2017). Our combined potential is the static Milky Way potential and the moving LMC potential. Next we look at adding the satellites in orbit around the LMC.

2.2 LMC Dwarfs

In this section, we explain how we populate the satellites around the LMC. We use the semi-analytic model `Galacticus` (Benson 2011) to model an LMC mass analog and its satellite population using merger trees derived statistically using Extended Press-Schechter.

`Galacticus` is a type of semi-analytical model solving galaxy formation physics within the current standard cosmological framework (Benson 2011). This model starts with the initial state of the universe and evolves it forward to look at galaxy properties. Properties computed include the mass of stars and gas in a galaxy, broad structural properties, dark matter contents, and observable quantities like luminosities, metallicities, chemical compositions, ect. (Benson 2011).

Extended Press Schechter (EPS) theory is another method used to efficiently generate merger trees. EPS theory approximates the mass functions of virialized dark matter halos from the density field statistics. The reasoning behind this theory is that if the

density is above some threshold, virialized structures will form. It is an extension from the work of Press & Schechter (1974). The EPS method uses a Monte Carlo Algorithm that will statistically populate a merger tree and are significantly more efficient than N-body simulations. EPS trees do have the drawback of being unreliable for halos that are $< 10^{10} M_{\odot}$ due to the dynamic range limitations of EPS (Somerville & Primack 1999).

The astrophysical prescriptions and parameters used in our LMC runs are based on those tuned in Weerasooriya et al. (2023) to reproduce the Milky Way satellites and that are also able to reproduce the known properties of the satellites of Centaurus A (Weerasooriya et al. 2023). Weerasooriya et al. (2023) uses the Galacticus semi-analytical model (SAM) running a model of high resolution merger trees from a cosmological N-body simulation to reproduce Milky Way dwarfs and used parameters that best fit observed luminosity functions and luminosity metallicity relations of Milky Way dwarfs.

In our LMC analogs we have incorporated two additional pieces of physics developed in Ahvazi et al. (2023), cooling via molecular hydrogen, and orbital tracing of satellite galaxies after infall. Ahvazi et al. (2023) built on the astrophysical prescriptions and parameters developed in Weerasooriya et al. (2023) and used EPS to generate a large number of merger trees of Milky Way, Centaurus A and LMC analogs, while fully resolving halos hosting the lowest mass galaxies.

The physics of H_2 cooling is significant for the modeling of star formation in low mass halos, as it allows gas in a halo to condense and form stars at lower dark matter masses (Ahvazi et al. 2023, Bovill & Ricotti 2009). This is especially important when modeling the dwarf satellites of dwarf galaxies since the satellites of dwarfs have lower dark matter masses (Mateo et al. 1998, Kleyna et al. 2001, Wilkinson et al. 2006).

For this work, the addition of orbital tracing of dark matter subhalos after infall in EPS trees in Ahvazi et al. (2023) is the most critical addition. At the moment when a dark matter halo infalls into a more massive galaxy, they draw an initial position and velocity statistically from the `Multidark-Galaxies` N-body simulations (Knebe et al. 2018). From that point on, the orbit is integrated in the potential of the host halo. As a result of this addition to Ahvazi et al. (2023) we are able to combine the position and velocity information of merger trees from an N-body simulations with the efficiency of merger trees generated by EPS. For satellites of the LMC from Ahvazi et al. (2023), we are looking at luminous satellites with mass $M_{sat} > 10^2 M_{\odot}$.

Additional details about the modeling of the baryonic properties of the dwarfs in Weerasooriya et al. (2023) and Ahvazi et al. (2023) and the orbital evolution developed in Ahvazi et al. (2023) can be found in their respective papers and formed the bulk of two doctoral theses and is beyond the scope of this work.

In this work, we use a set of five LMC analogs with a range of masses (Table 2.1) run for us by Niusha Ahavzi (UC Riverside/Carnegie Observatory) with a resolution of $10^7 M_{\odot}$. We then select the luminous satellites from the LMC analogs and extract their positions and velocities. For the remainder of this work we consider the LMC analog with $M = 1.32 \times 10^{11} M_{\odot}$ as our fiducial model as it best corresponds to estimates of the LMC mass Erkal et al. (2019).

The satellites of the LMC analog will be treated as test particles in the combined potential of the Milky Way and the moving LMC. For our model, we are looking at the UFD LMC satellites that have a mass range of $10^2 - 10^5 M_{\odot}$ (Richstein et al. 2024).

Doing this significantly simplifies our models while returning a good approximation of each of the satellites and for the LMC satellites $M_{satellite} \ll M_{LMC} < M_{MW}$.

2.2.1 And Around It Goes...

We now can select a sample of LMC satellites for a given LMC mass and put them in orbit around the LMC. However, we're still faced with one uncertainty, the orientations of these satellites during infall. Given we have the necessary parameters to calculate their positions and velocities, we can solve for their initial radial distance, velocity, and orientation. This does not mean that these are each satellite's orientations over the past 6 Gyr. To solve this, we will introduce a randomized rotation to each satellite's orientation.

With our initial 6-D positions and velocities of our sample determined, we introduce a rotation to each of our sample satellites. This will allow us to find a distribution of positions and distances of our LMC satellites. First, we must convert our satellite's position in (x, y, z) and velocity in (v_x, v_y, v_z) , pulled from the works of Ahvazi et al. (2023). This process is illustrated as the first step in Figure 2.5. Then we convert from Cartesian to spherical coordinates to find their initial Galactocentric distance (r_{GC} and $v_{r_{GC}}$) and their orientations as ϕ_0 and θ_0 . The conversions for position and velocity we used are as follows:

$$r_{GC} = \sqrt{x^2 + y^2 + z^2} \quad (2.10)$$

$$\phi_{0r} = (\text{sign}(y)) \arccos\left(\frac{x}{\sqrt{x^2 + y^2}}\right) \quad (2.11)$$

$$\theta_{0r} = \begin{cases} \arctan\left(\frac{\sqrt{x^2+y^2}}{z}\right) & \text{for } z > 0 \\ \pi + \arctan\left(\frac{\sqrt{x^2+y^2}}{z}\right) & \text{for } z < 0 \end{cases} \quad (2.12)$$

$$v_{RGC} = \sqrt{v_x^2 + v_y^2 + v_z^2} \quad (2.13)$$

$$\phi_{0v} = (\text{sign}(v_y)) \arccos\left(\frac{v_x}{\sqrt{v_x^2 + v_y^2}}\right) \quad (2.14)$$

$$\theta_{0v} = \begin{cases} \arctan\left(\frac{\sqrt{v_x^2+v_y^2}}{v_z}\right) & \text{for } z > 0 \\ \pi + \arctan\left(\frac{\sqrt{v_x^2+v_y^2}}{v_z}\right) & \text{for } z < 0 \end{cases} . \quad (2.15)$$

We first must calculate r_{GC} and $v_{r_{GC}}$ from the satellite's 3-D positions and velocities. This is necessary for calculating our ϕ_0 and θ_0 values. Calculating ϕ_0 has no component in position or velocity in the z-direction, having a full rotation around the x-y plane from 0 to 2π . ϕ_0 orientation is dependant on the sign of the y-component in position and velocity and will determine if our ϕ_0 value is positive or negative. Our calculation for θ_0 is a little more complicated. The equation used to calculate θ_0 is dependant on the value of z. For positive values of z, the calculation is fairly straightforward. However, for negative values of z we must add a π to the final result. Without this correction, conversion into other coordinates will not work properly. This process is illustrated as the second step in Figure 2.5.

Now that we have our initial positions and velocities in spherical coordinates, we can introduce to each satellite a randomized rotation ($d\phi$ and $d\theta$) by generating a random number in python. The values of $d\phi$ and $d\theta$ are added to ϕ_0 and θ_0 to give us new values (ϕ_{new} and θ_{new}). These values are then used with our r and v values from above to recalculate the 3-D positions and velocities, converting from spherical coordinates back

to Cartesian coordinates. Using the new rotation values will change to 3-D positions and velocities of our satellites, allowing us to investigate what happens in their orbits. These are calculated from the following spherical-to-Cartesian equations.

$$x = r \cos(\phi_0 + d\phi) \sin(\theta_0 + d\theta) \quad (2.16)$$

$$y = r \sin(\phi_0 + d\phi) \sin(\theta_0 + d\theta) \quad (2.17)$$

$$z = r \cos(\theta_0 + d\theta) \quad (2.18)$$

$$v_x = v \cos(\phi_0 + d\phi) \sin(\theta_0 + d\theta) \quad (2.19)$$

$$v_y = v \sin(\phi_0 + d\phi) \sin(\theta_0 + d\theta) \quad (2.20)$$

$$v_z = v \cos(\theta_0 + d\theta). \quad (2.21)$$

The equations above use the notation $\phi_0 + d\phi$ and $\theta_0 + d\theta$, which is equivalent to our ϕ_{new} and θ_{new} . These return our new values for 3-D positions and 3-D velocities $(x_{new}, y_{new}, z_{new}, v_{x_{new}}, v_{y_{new}}, v_{z_{new}})$. This process is illustrated as the third step in Figure 2.5.

We took our new 6-D in Cartesian space and converted them to cylindrical coordinates using a Cartesian to cylindrical conversion package in Galpy. This is necessary to do for us to run the orbital integral in Galpy (Bovy 2015). The conversions from Cartesian to cylindrical and cylindrical to Cartesian coordinates are provided for completion.

$$r = \sqrt{x^2 + y^2} \quad (2.22)$$

$$\theta = \arctan\left(\frac{y}{x}\right) \quad (2.23)$$

$$z = z \quad (2.24)$$

$$x = r \cos(\theta) \quad (2.25)$$

$$y = r \sin(\theta) \quad (2.26)$$

$$z = z. \quad (2.27)$$

Galpy allows us to run an orbit integration to return out values of 3-D position, 3-D velocity, and ϕ (Bovy 2015). This process is illustrated as the fourth step in Figure 2.5. We take these values and convert them back into Cartesian coordinates using a cylindrical to Cartesian conversion package in Galpy (Bovy 2015). This rotation process is repeated over 100 randomized rotations, giving all of our subjected satellites 100 different randomized rotations to build our statistics as illustrated in the fifth step in Figure 2.5. This will give us an overall distribution that we can project and analyze the results. We will also be able to look at their Galactocentric distances and determine if they are potentially visible for observation.

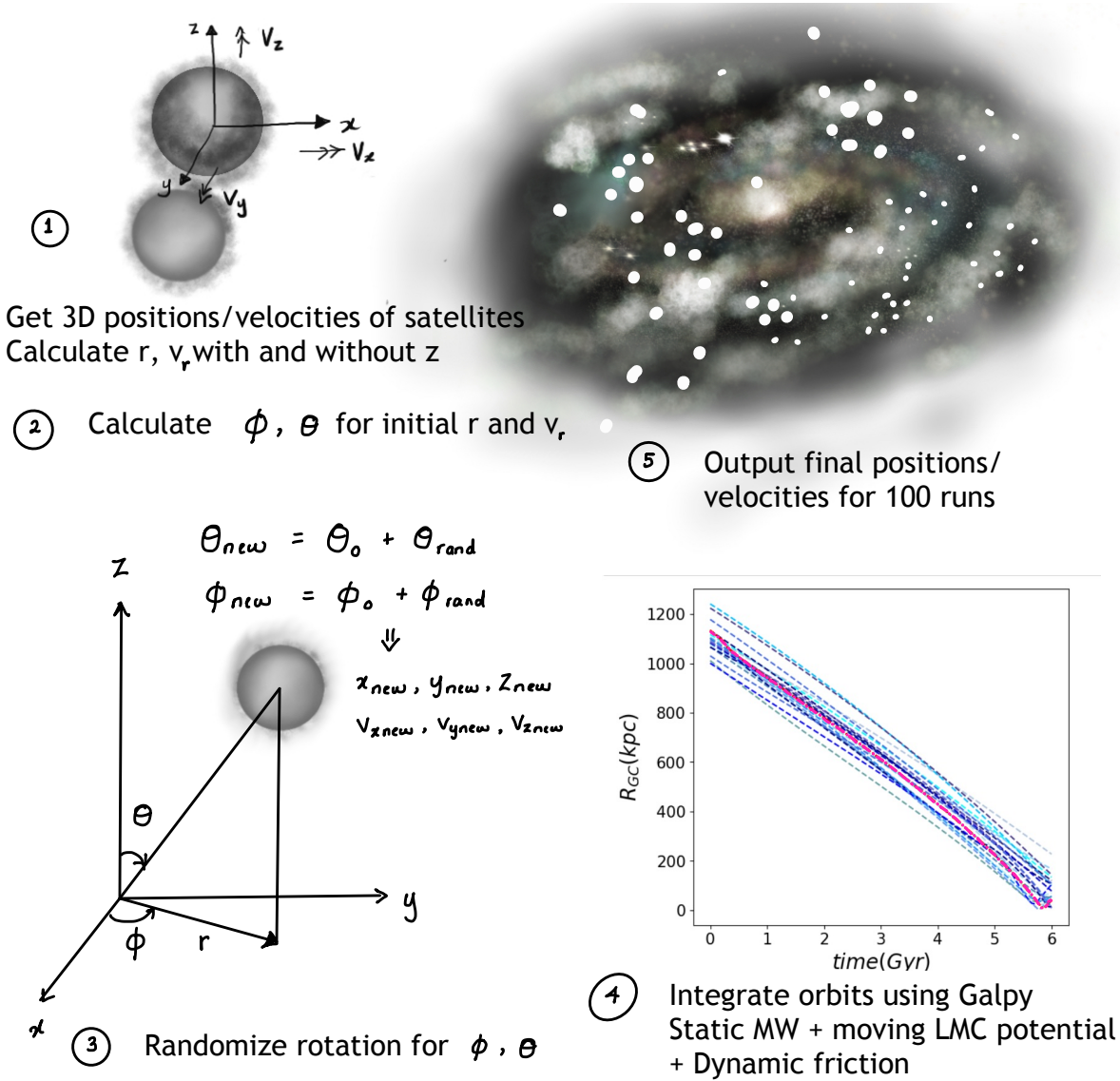


Figure 2.5: Diagram of our randomized rotation process. The process is as follows. 1) Get the initial 3-D positions and velocities of our satellites and calculate their respective R_{GC} , V_r , and z values with and without z . 2) Calculate the initial ϕ and θ from our values of R_{GC} and V_r . 3) Add a randomized rotation ($d\phi$ and $d\theta$) to our initial ϕ_0 and θ_0 . 4) Integrate the orbits of our satellites using the orbital function of Galpy for our combined static MW, moving LMC, and df potential. 5) This process is repeated for each satellite 100 times to build statistics to find the overall distribution of our LMC satellite sample.

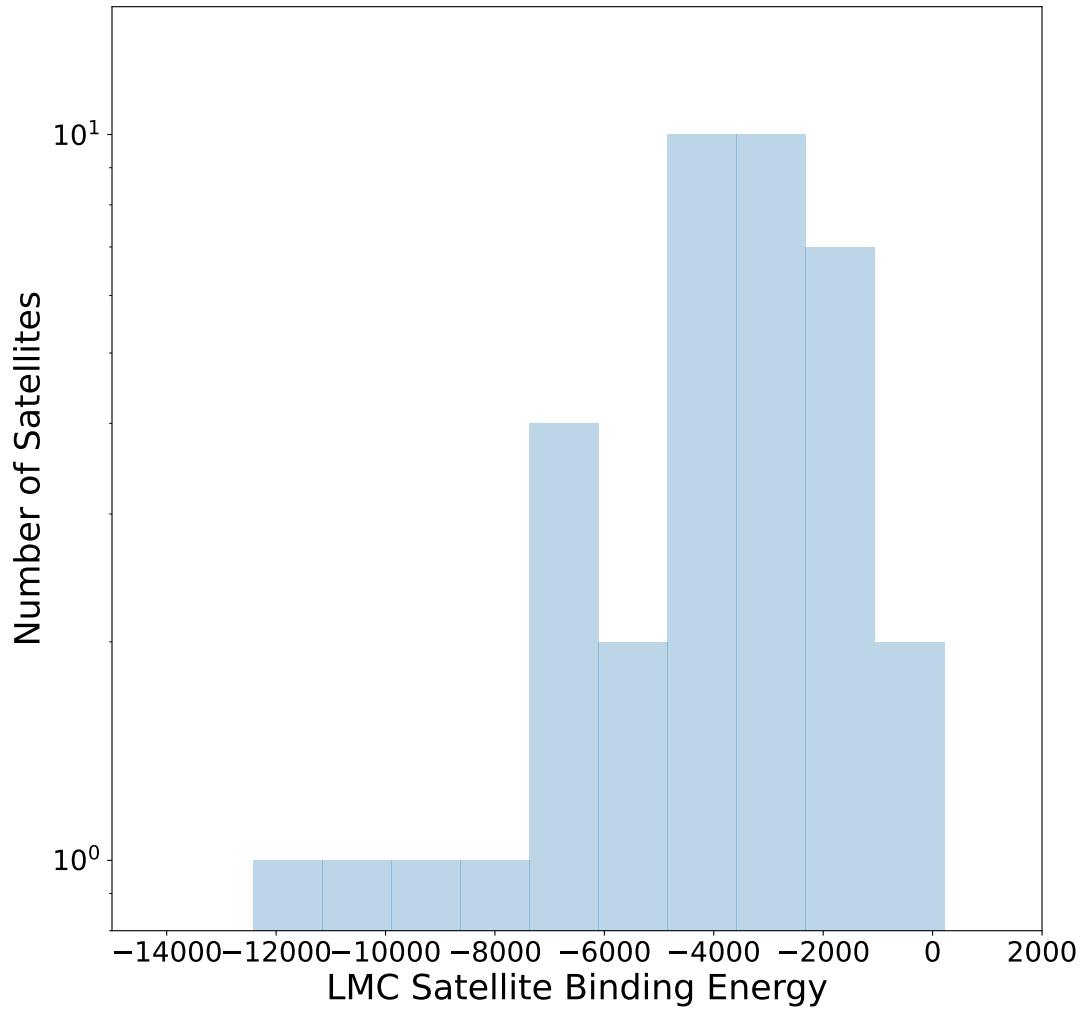


Figure 2.6: Histogram of the initial binding energies of LMC satellite sample. This histogram shows the number of satellites with those specific binding energies. We can see that most of these satellites are bound to the LMC. We will explore in Figure 2.9 the correlation between distances of the LMC satellites from the LMC and how strong a satellite’s binding energy is. Conventions and explanations in this plot will hold true for the other distance comparison plots.

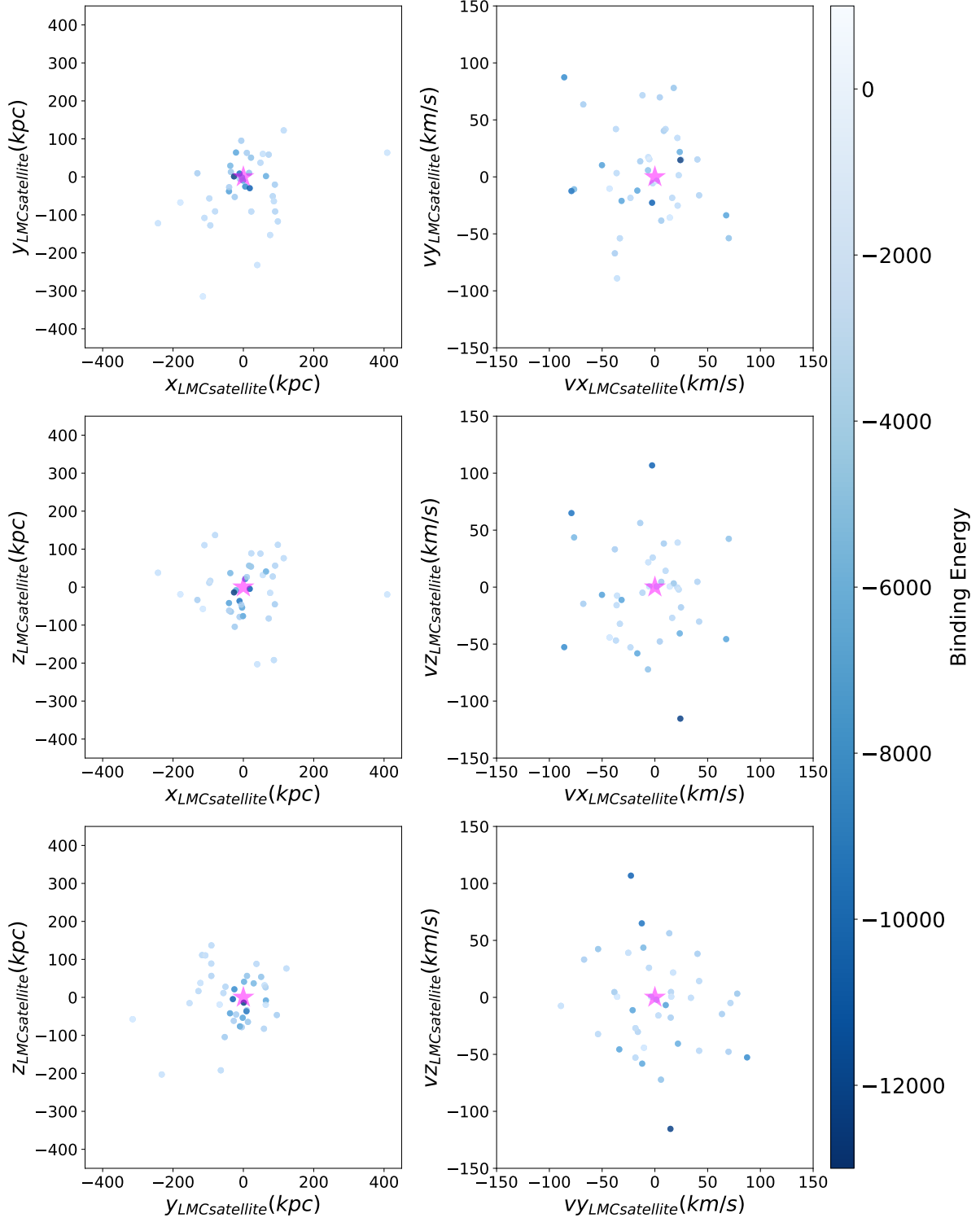


Figure 2.7: Above is six figures of our LMC satellite sample’s positions (left panels in kpc) and velocities (right panels in km/s) at first infall. The LMC is centered at (0,0) and represented by a fuchsia star. All of our LMC satellites are color coded based on their binding energy to the LMC. For the positions of LMC satellites, we find the more bound satellites are closer to the LMC (where the LMC is at the 0 position in x, y, and z). These conventions will hold true for the rotated and shifted figures.

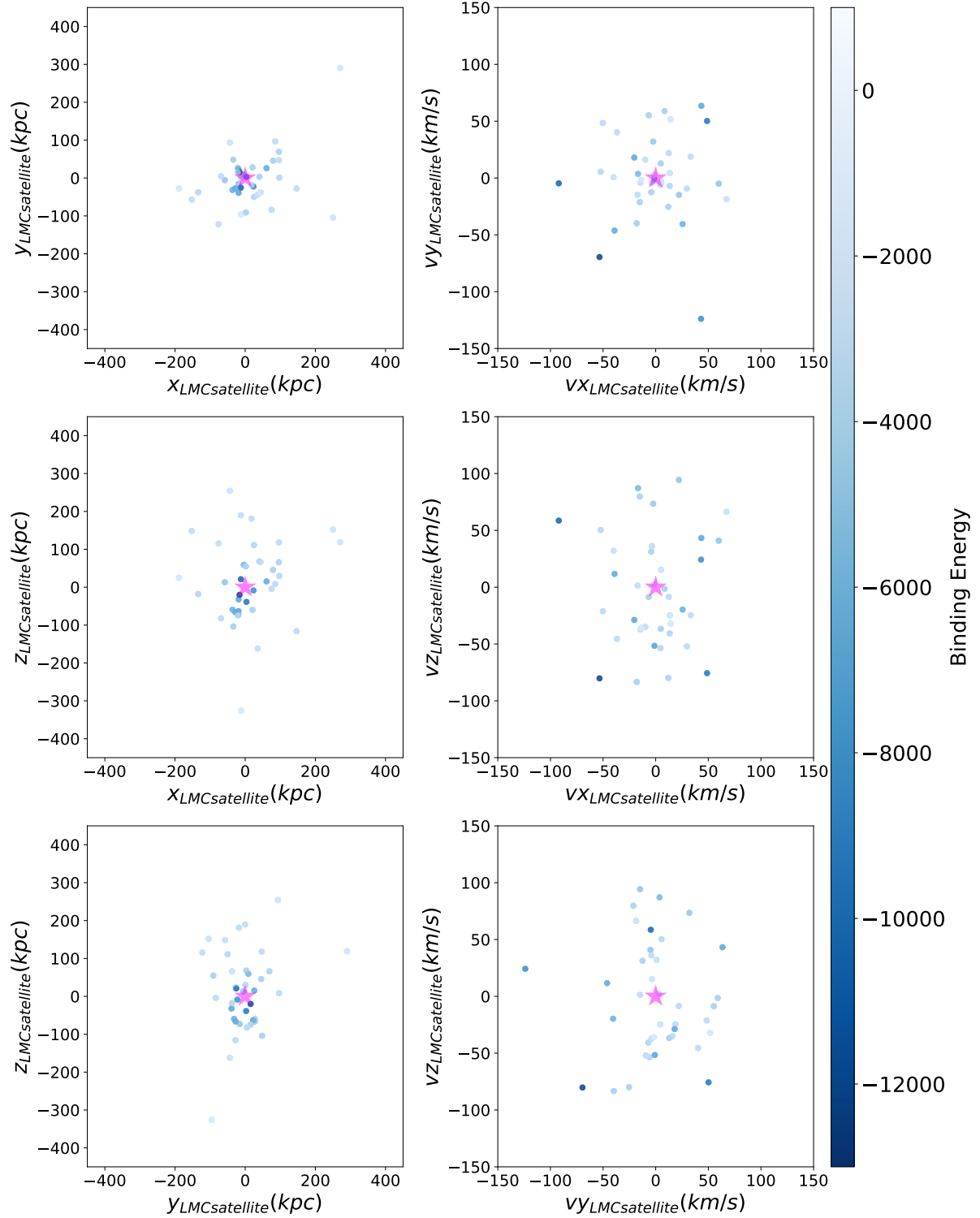


Figure 2.8: Above is the six figures after we introduce the randomized rotation to the satellites. Plot layout is the same as in Figure 2.7. The randomized rotation introduces new positions and velocities to our LMC satellite sample, but we see that they are still centered around the LMC.

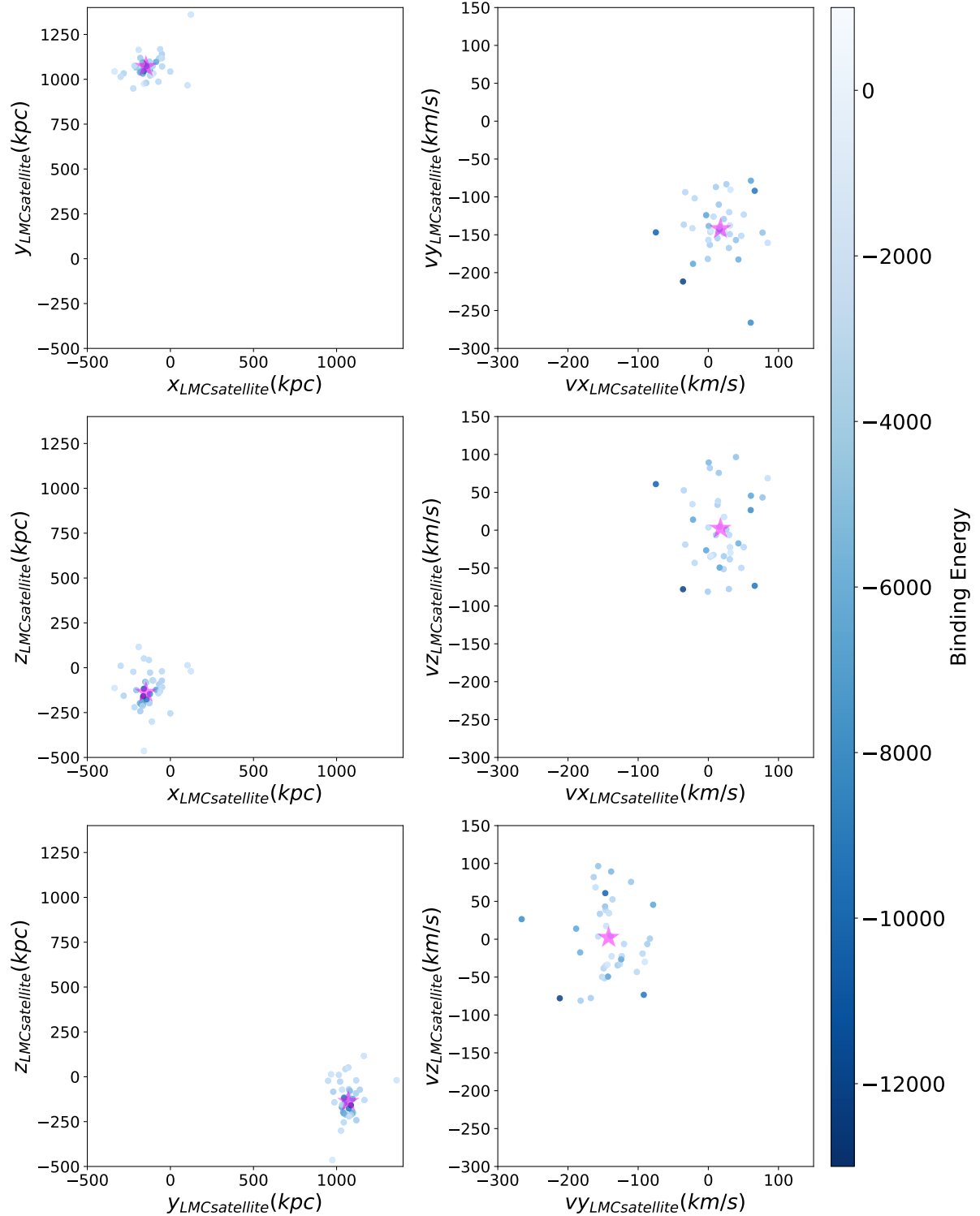


Figure 2.9: Above is the six figures after we add the randomized rotation to our initial rotations and evolved backwards by 6 Gyr. Plot layout is the same as in Figure 2.7. The positions of our LMC satellite sample is shown to shift back to their distances around the LMC 6 Gyr ago. However, we see that they are still centered around the LMC after evolving backwards by 6 Gyr, giving us our LMC satellite's initial 3-D positions and 3-D velocities.

In Figure 2.7, we show our LMC satellites present day 3-D Cartesian positions (left panel) and velocities (right panel) pulled from the work of Ahvazi et al. (2023). Our satellites are colored based on their binding energy to the LMC with the LMC centered at (0,0) represented by a fuchsia star. The binding energy is calculated as follows

$$BE_{sat} = KE_{sat} + GE_{sat}, \quad (2.28)$$

where KE_{sat} and GE_{sat} are the kinetic and gravitational energies of the satellites given as

$$KE = \frac{1}{2}v^2 \quad (2.29)$$

$$GE = \frac{-GM_{LMC}}{r}. \quad (2.30)$$

G is the gravitational constant ($G = 4.3009 \times 10^{-6} \text{ kpc } M_{\odot}^{-1} (\text{km/s})^2$), M_{LMC} is the mass of our fiducial LMC ($M_{LMC} = 1.32 \times 10^{11} M_{\odot}$), r is the Galactocentric distance from equation (2.10), and v is the radial velocity from equation (2.13) above. The binding energy is based on a gravitational two-body problem between the LMC satellites and the LMC potential with units of km^2/s^2 . Figure 2.6 displays the binding energies of our sample satellites, showing that most of the satellites are bound to the LMC.

For our positions, we find our higher binding energy satellites are closer to the LMC in our 3-D space. This shows that the LMC satellites that are more bound tend to be closer to the LMC. The further out from the LMC our LMC satellites are, the less bound they are to the LMC, making them more likely to be captured or become unbound when interacting with a larger galaxy like during the first infall into the Milky Way. In order to

get the satellites positions and velocities around the LMC back 6 Gyr, we must introduce the randomized rotation. We can see that the introduction of the randomized rotation changes the satellites positions and velocities shown in Figure 2.8. The satellites stay centered around the LMC in their new positions. Finally, we must evolve time for our satellites orbiting the LMC back 6 Gyr to find their positions and velocities. We see in Figure 2.9 that the satellites positions and velocities change to larger values, indicating they are farther away and moving faster than present day. Even with an evolution in time of 6 Gyr, they remain in orbit around the LMC as the LMC marker remains in the center back 6 Gyr ago. Next, we can look at how we send our LMC potential with it's orbiting satellite sample back 6 Gyr into the Milky Way.

2.3 Into the Milky Way

Now that our model is set up and everything is in the right place, we can evolve the LMC with it's orbiting satellites forward by 6 Gyr, sending it into the Milky Way. As our model evolves forward by 6 Gyr, we can look at the orbital parameters using the orbital integration package from Galpy Bovy (2015). This is done by using a cylindrical coordinate system from the Galactocentric center in the x-y plane of the Milky Way disk in four dimensional space (three dimensions of space and one dimension of time). This is shown in Figure 2.9 with the shift of position and velocity back 6 Gyr. We then evolve the orbits of our satellites as test particles in our moving potential in Galpy. Our new positions and velocities can be converted to be projected to show our distribution in Galactic latitude and longitude.

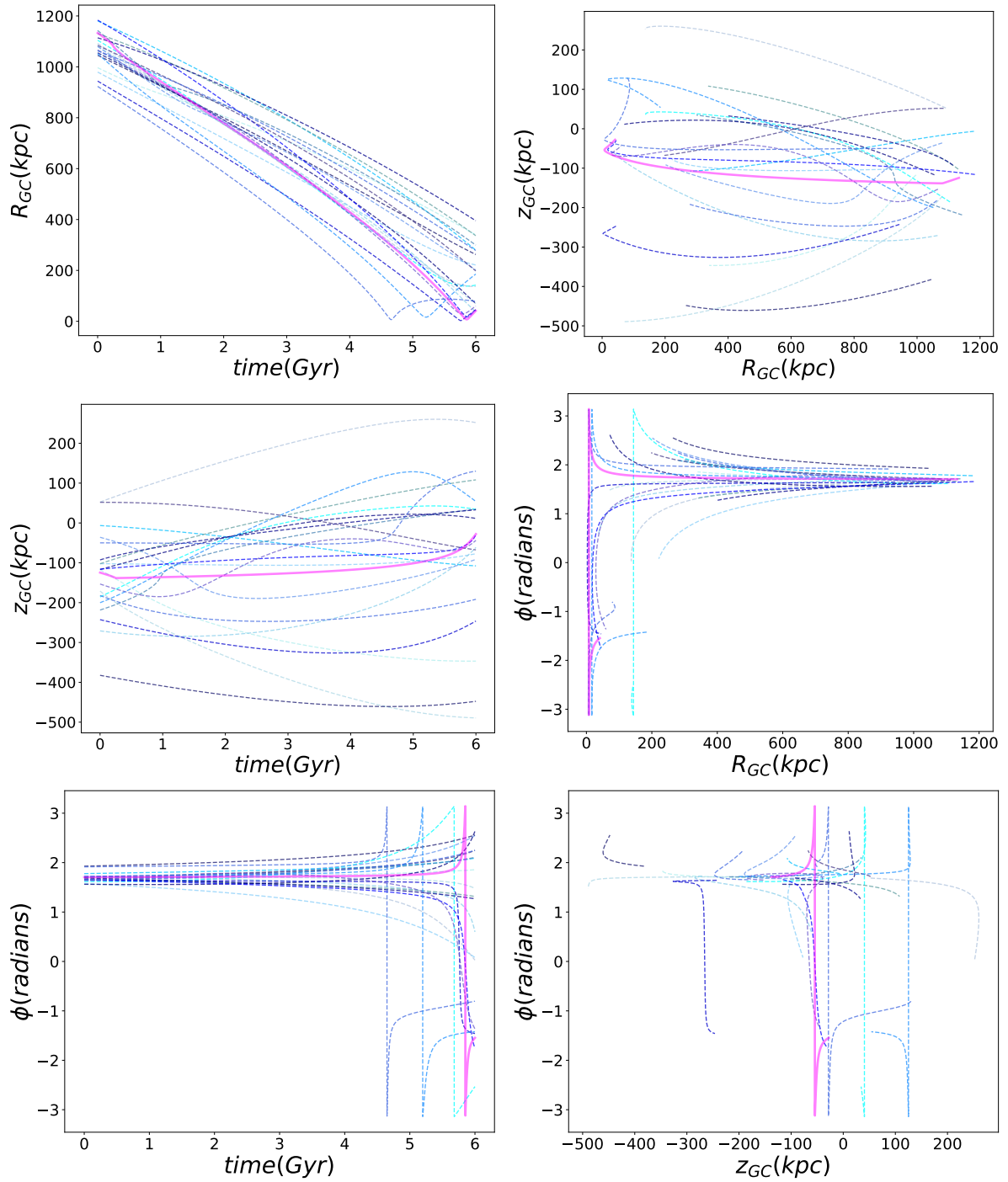


Figure 2.10: We have six different plots of our LMC satellite sample's orbital parameters in cylindrical coordinates. All the left panel plots will be time in Gyr versus R_{GC} in kpc (top left), z_{GC} in kpc (middle left), or ϕ in radians. The right panels compare our R_{GC} , z_{GC} , and ϕ against each other. Each 'blue' colored dashed line represents one of our LMC satellite's orbits with the LMC's orbit represented by the fuchsia dotted-dashed line for reference.

In Figure 2.10 we show six plots of our LMC satellite's parameters in cylindrical coordinates and time. All the plots on the left panel are time (Gyr) versus Galactocentric distance (R_{GC} (kpc)), position above/below the Milky way disk (z_{GC} (kpc)), and the azimuth (ϕ (Radians)). The plots on the right panel compare our three cylindrical parameters against each other. R_{GC} , z_{GC} , and ϕ . Each 'blue' colored dashed line represents one of our LMC satellite's orbits with the LMC's orbit represented by the fuchsia solid line for reference. The plots look at time versus Galactocentric distance (top left), time versus Galactocentric distance above or below the Milky Way disk (middle left), time versus azimuthal (bottom left), Galactocentric distance versus Galactocentric distance above or below the Milky Way disk (top right), Galactocentric distance versus azimuthal angle (middle right), Galactocentric distance above/below the Milky Way disk versus azimuthal angle (bottom right). We can see that many of the LMC satellites follow the LMC path and leave with the LMC in the time versus Galactocentric distance and Galactocentric distance above/below the Milky Way disk. These satellites are going through first infall with the LMC. Some satellites have oscillatory patterns around the LMC orbit, showing that they are in orbit and bound to the LMC. Other satellites that are further away from the LMC's orbit do not have similar paths to the LMC, indicating they are no longer in orbit with the LMC. The plots with ϕ have asymmetric behaviors as their values flip from positive to negative. This is showing that they are going into orbit with the Milky Way.

Chapter 3

Observations

In this chapter, we describe the observational sample of Local Group dwarfs that are either confirmed or potential satellites of the LMC. These are the dwarfs to which we will compare our models.

3.1 Local Group Dwarfs

First, we need to differentiate between dwarf satellites of the Milky Way and dwarf satellites that were originally orbiting the LMC. To do this, we look at the the current data for the Local Group Dwarfs (McConnachie 2012) and using Erkal & Belokurov (2020), Patel et al. (2020), Vasiliev (2023) among others, we determine which dwarfs are known and suspected LMC dwarf satellites.

Determining LMC dwarf candidacy has been done in a number of ways. Works done by Kallivayalil et al. (2018) and Patel et al. (2020) looked at dwarf galaxies using the GAIA Data Release 2 (DR2). Membership selection of LMC dwarf satellites was based on Proper Motions and positions in the Color-Magnitude Diagram (CMD) from the GAIA DR2 survey that were within three times of the half-light radii of each dwarf galaxy (Kallivayalil et al. 2018). With the GAIA DR2, measurements of Proper Motions and radial velocity of the lowest-mass ultra faint satellites are used to calculate the orbital histories of 13 UFD satellites in a combined MW/LMC/SMC potential (Patel et al. 2020). Magellanic satellites compared CMD and Star Formation History (SFH) to determine the compatibility of being Magellanic system satellites Sacchi et al. (2021). The release of GAIA Data Release 3 (DR3) allowed for even more dwarf galaxies to be analyzed for LMC candidacy Battaglia et al. (2022)

Estimates for the number of UFD satellites ($M = 10^2 - 10^5 M_{\odot}$) orbiting the LMC vary between different works. Kallivayalil et al. (2018) estimated between 5 - 40 UFD satellites be found orbiting the LMC where Patel et al. (2020) predicted 5 - 10 UFD's to be found orbiting around LMC. Erkal & Belokurov (2020) used the predicted number of satellites (70^{+30}_{-40}) for a magnitude range of -7 to -1 as a reference. Their calculations estimate around 60 UFD satellites should be orbiting around the LMC.

The list of suspected and confirmed satellites based on current literature is shown in Table 3.1. Additionally, we compare works candidacy findings in Table 3.2

Table 3.1: Known and Suspected LMC Satellites

Galaxy Name	Galactic Latitude (l)	Galactic Longitude (b)
Confirmed LMC Satellites		
Carina 2	6.1286	-0.9065
Carina 3	4.7366	-0.9553
Hydrus 1	5.6494	-1.0428
Phoenix 2	4.6477	-0.8681
Grus 2	5.4679	-0.9650
Horologium 1	4.7121	-0.2991
Reticulum 2	4.7125	-0.2940
Tucana 4	5.1909	-0.6413
Suspected LMC Satellites		
Tucana 3	1.7156	4.7989
Segue 1	4.7989	-1.0402
Aquarius 2	5.5044	-0.9806
Canes venatici 2	0.9618	-0.9252
Draco 2	1.9823	1.4434
Eridanus 3	3.8481	0.8801

Table 3.2: LMC Satellite candidacy based on the works of Sales et al. (2017) [S17], Kallivayalil et al. (2018) [K18], Erkal & Belokurov (2020) [E/B20], Patel et al. (2020) [P20], and Battaglia et al. (2022) [B22]. Satellite’s candidacy is given by highly likely (+), unlikely (-), uncertain (?), and recently captured/interacting satellites (c). Brackets around the recently captured/interacting satellites are identified as Milky Way satellites that have close encounters with the LMC, but remain satellites of the Milky Way.

Galaxy Name	S17	K18	E/B20	P20	B22
Carina 2		+	+	+	+
Carina 3		+	+	+	+
Hydrus 1		+	+	+	+
Phoenix 2	?	?	+	c	+
Grus 2			-		c
Horologium 1	+	+	+	+	+
Reticulum 2	?	-	+	c	+
Tucana 3		-	-	[c]	-
Tucana 4	?		-	?	?
Segue 1			-	[c]	-
Aquarius 2		-		[c]	-
Canes venatici 2			-	-	-
Draco 2	?	?		-	
Eridanus 3	?		?		

In Figure 3.1, we project the known/suspected LMC dwarf satellites (in red) onto an Aitoff projection in Galactic coordinates in addition to all Milky Way dwarf satellites (in grey). The locations of the LMC and SMC are shown as stars for reference (Black stars

with red outline). We note, that the majority of the current known and suspected LMC satellites are in vicinity of the LMC and SMC or near the Magellenic Stream (Kallivayalil et al. 2018). For reference, the velocity vectors of all satellites including the LMC and SMC are placed on the Aitoff projection.

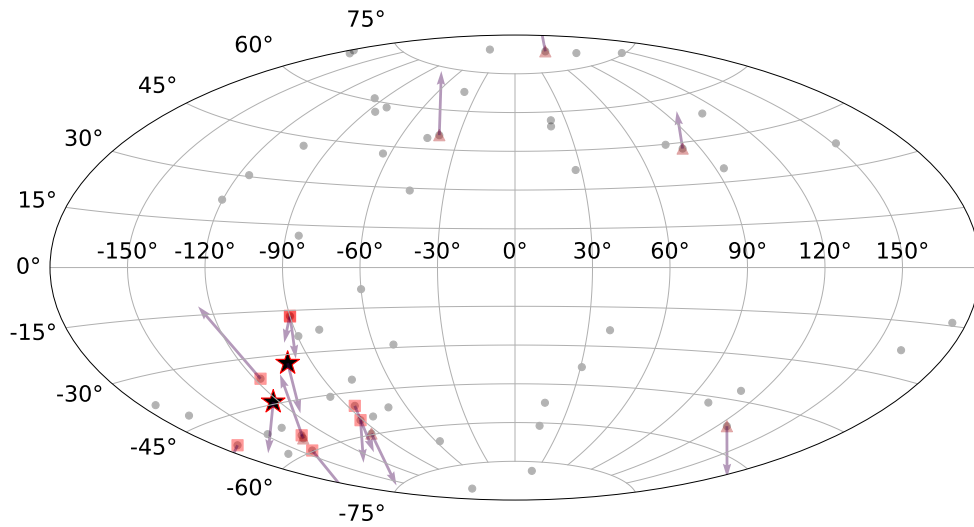


Figure 3.1: Projection of all known MW satellites (black circles) in Galactic latitude and longitude. Plotted are the known and suspected LMC satellites (red squares and maroon triangles) along with the LMC and SMC (Black stars with red outline). The LMC, SMC, the known, and suspected satellites have their velocity vectors for reference of each galaxy’s direction.

Many dwarf galaxies have been studied for their potential candidacy as satellites of the LMC. Table 3.2 illustrates the satellite candidacy results across multiple works. It

is widely accepted that Carina 2, Carina 3, Horologium 1, and Hydrus 1 are likely UFD members of the LMC. The work of Kallivayalil et al. (2018) looked at Carina 2, Carina 3, Horologium 1, and Hydrus 1 and were the first confirmed of type of satellite infall predicted by Λ CDM theory. These were determined by the radial velocity measurements from GAIA DR2 to get their 3-D kinematics of the UFDs (Patel et al. 2020, Erkal & Belokurov 2020, Sacchi et al. 2021). Patel et al. (2020) identified the UFD Crater 2, Carina 2, Carina 3, Hydrus 1, Horologium 1, Reticulum 2, Tucana 3, Seque 1, Aquarius 2, Canes Venatici 2 to have a $\geq 50\%$ probability of being members based on the Vast Polar Structure (VPOS). They determined Carina 3, Horologium 1, Hydrus 1, and Phoenix 2 to be long-term Magellanic satellites. Erkal & Belokurov (2020) integrated 25 UFD orbits backwards by 5 Gyr to determine that Carina 2, Carina 3, Horologium 1 are likely LMC members. The works of Sacchi et al. (2021) further confirmed that Carina 2, Carina 3, Horologium 1, Hydrus 1 are UFD satellites compatible with LMC debris from GAIA DR2. In addition, Reticulum 2 and Phoenix 2 are determined to be members of the Magellanic system (Erkal & Belokurov 2020). Carina 2, Carina 3, and Hydrus 1 are LMC satellites, confirmed using the GAIA DR3 (Battaglia et al. 2022). Further, Carina 2 and Reticulum 2 are used to look at their proper motion and Color Magnitude Diagram to compare the likeliness of being Magellanic system satellites for those UFDs (Kallivayalil et al. 2018, Alexander et al. 2023).

Satellites that have potential LMC candidacy were studied in Kallivayalil et al. (2018), Patel et al. (2020), Erkal & Belokurov (2020). Hydra 2, Draco 2, Tucana 2, and Grus 1 have possible association with the Magellanic system. Hydra 2, Draco 2, Tucana 2, and Grus 1 had consistent 6-D measurements within 1σ of error for their orbital

poles, but required more detailed orbital modeling to confirm Kallivayalil et al. (2018). Additionally, Erkal & Belokurov (2020) found that Horologium 2 and Tucana 4 have modest probabilities of being LMC satellites.

Some satellites were recently captured by the LMC. Reticulum 2 and Phoenix 2 were recently captured Magellanic satellites (Patel et al. 2020, Vasiliev 2023). Patel et al. (2020) found that Reticulum 2 and Phoenix 2 had to be recently captured since they have only completed one orbit around the Magellanic Clouds in the last 1 Gyr. Battaglia et al. (2022) further concluded these findings with better systematic PMs leading to stronger correlation based on higher probabilities. Reticulum 2 and Phoenix 2 have LMC association using the GAIA DR3 (Battaglia et al. 2022). Grus 2 had an orbit that clearly shows it did not originate in the Magellanic system, but was captured in the last 200 Myr (Battaglia et al. 2022). Tucana 4 is potentially parented by the LMC, captured 500 Myr ago (Battaglia et al. 2022)

Some satellites were found to be unlikely candidates of the LMC. Kallivayalil et al. (2018) Tucana 2, and Grus 1 have velocity components that were inconsistent with their 3σ predictions. Patel et al. (2020) used more detailed orbital models of Hydra 2 and Draco 2 to explore candidacy presented in Kallivayalil et al. (2018). They found no association between these two dwarf satellites and the Magellanic Clouds. Erkal & Belokurov (2020) calculated probabilities of being LMC satellites for the dwarfs studied in a Milky Way/LMC system. Tucana 2, Reticulum 3 and Hydra 2 were found to be unlikely LMC candidates Erkal & Belokurov (2020), Vasiliev (2023).

In Figure 3.2, we show the distribution of the Milky Way satellite's Galactocentric distance in kpc. The dashed line placed at 150 kpc represents satellites that are poten-

tially visible from Earth from current surveys like GAIA. We use this marker to check the distribution of the known and suspected LMC satellites distances from Earth. We plot the known Milky Way satellites (grey) in the background and place the known LMC satellites and suspected LMC satellites (red) from the our discussion above of LMC dwarfs. We show that most of the known and suspected LMC satellites are within ~ 150 kpc from the LMC. The known and suspected LMC satellites with references are provided in Table 3.1.

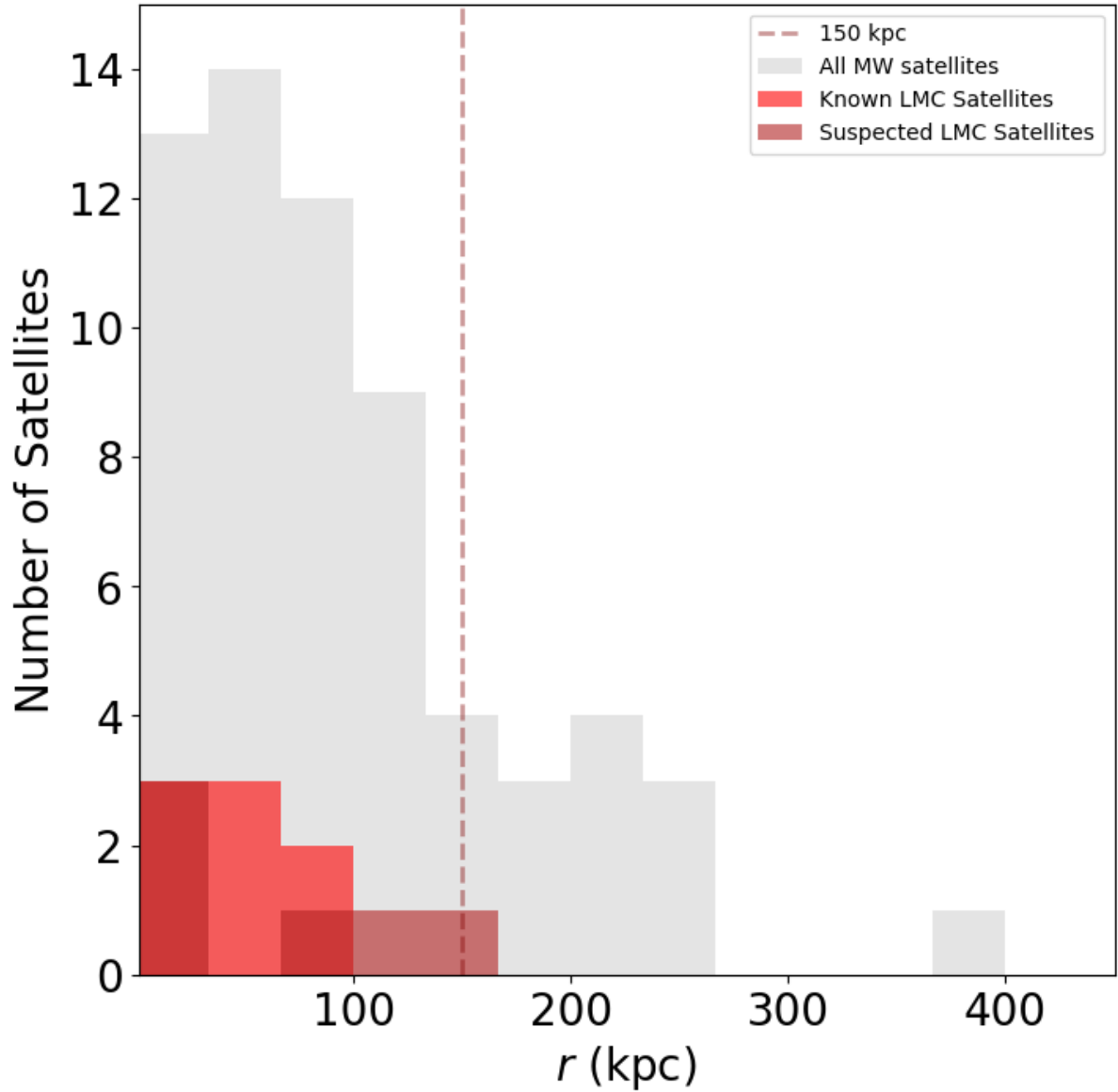


Figure 3.2: Histogram distribution of the number of satellites as a function of their Galactocentric distance (r) in kpc. Three different satellite classes are placed on histogram, known LMC satellites (red), potential LMC satellites (dark red), and all the Milky Way satellites (gray). The vertical red dashed line is set at 150 kpc to emphasize the distances from Earth the LMC's known and potential satellites are. At ~ 150 kpc from Earth, satellites have the potential to be detected by modern surveys like GAIA. Most of the potential and known satellites are within this 150 kpc distance cutoff.

Chapter 4

Results

In this chapter, we will discuss the results of our research. Using our model, we will look at our LMC satellite sample to determine where the LMC's missing satellites are.

4.1 Sample Projections

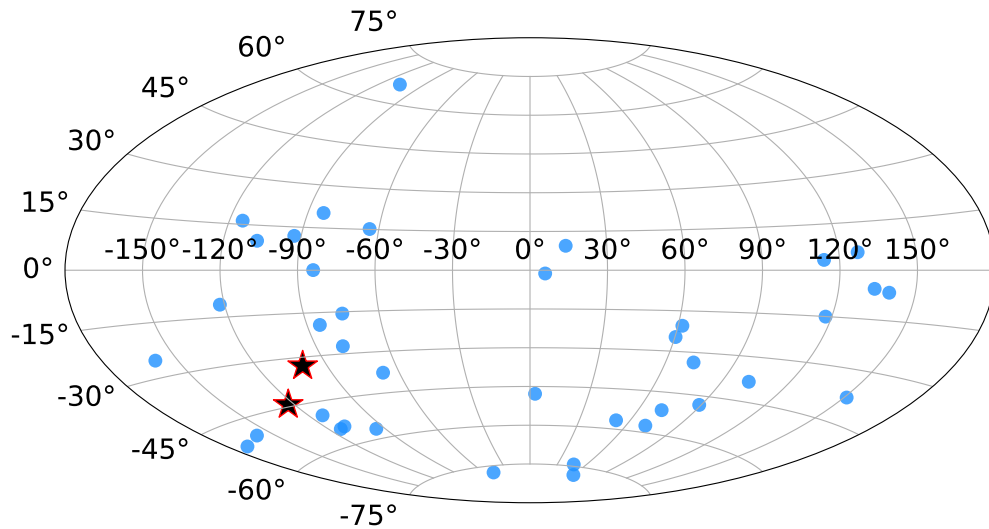


Figure 4.1: We tested one run of our selected sample satellites with randomized rotations through the moving LMC potential. These satellites are not subjected to any randomize rotation and are plotted based on their initial parameters. The final positions of each of our satellites are projected in Galactic latitude and longitude onto an Aitoff projection (blue circles). For reference, the LMC and SMC are projected as marked by the black stars outlined in red.

In Figure 4.1, we show the Aitoff projection of our sample satellites based on their initial parameters from the works of Ahvazi et al. (2023) (see section 2.2). The initial parameters

of our satellites are based on the model we use for our LMC ($M_{LMC} = 1.32 \times 10^{11} M_{\odot}$). For this initial run, none of the satellites are subjected to a random rotation of their ϕ or θ angles. Each satellite's three dimensional positions and velocities are converted from our 6-D Cartesian parameters (3 positions [x,y,z] and 3 velocities [v_x , v_y , and v_z]) to spherical coordinates to find our values of r, v, ϕ and θ . These values are used to convert from spherical coordinates back to our 6-D Cartesian parameters. We convert our 6-D Cartesian parameters into 6-D cylindrical parameters (3 positions [R, ϕ ,z] and 3 velocities [v_R , v_T , and v_z]) in order to run Galpy's orbital integration. Once the orbital integration is complete on the set, they are converted back into our original 6-D Cartesian parameters. Their respective 3-D positions Cartesian are then converted to Galactic latitude and longitude and their positions are plotted on an Aitoff projection (blue circles). Figure 4.1 plots our one run of our fiducial LMC potential with the LMC satellite sample. For reference, we include the positions of both the LMC and SMC as black stars outlined in red for a benchmark to compare against our model. Next we will look at the projection of our LMC satellites for 100 randomized rotations. This will help build our statistical analysis of our fiducial model.

4.1.1 100 Run Sample Projections

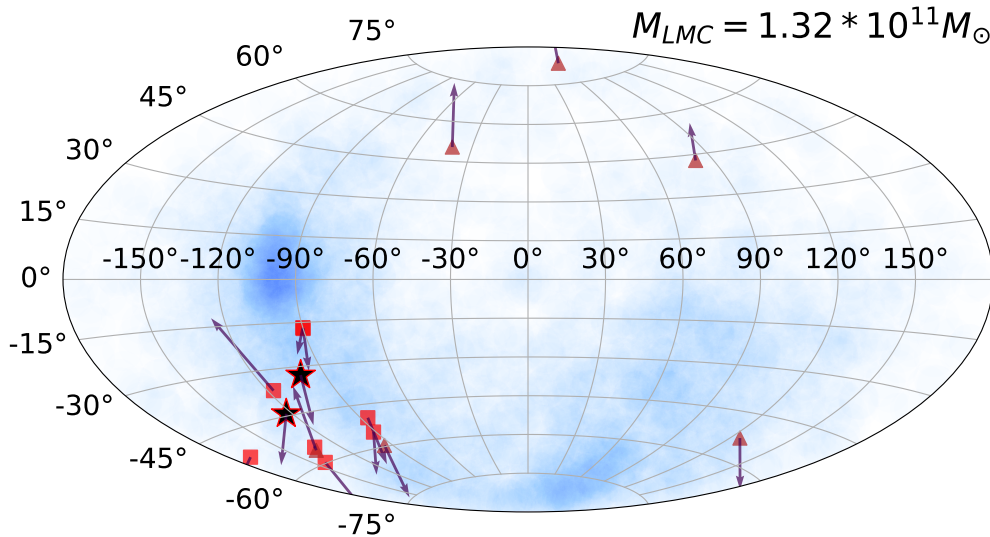


Figure 4.2: We continued by putting our selected sample through 100 runs, randomizing the angles of our θ and ϕ for each run past the initial run. The results are projected as a distribution (blue) similar to what we did in Figure 4.1. For reference, we plotted the positions of the LMC and SMC as stated before. Additionally, we plotted the known LMC satellites (red squares) and suspected LMC satellites (maroon triangles) with all markers having their velocity vector component added as a further reference. We see three areas of concentrated satellite distribution, near the LMC/SMC, above the LMC/SMC in the Galactic plane, and near the southern Galactic pole, in the Magellanic Stream.

In Figure 4.2, we show the results of 100 runs of randomized rotations of our LMC sample satellites. Our LMC satellites with 100 randomized rotations follow the same convention as we stated for the 1 run sample, using the LMC and the SMC as reference points

like in Figure 4.1. Added are the known/suspected LMC satellites (red squares/maroon triangles) gathered from chapter 3 on LMC Dwarfs for reference in our model. All known and suspected satellites have velocity vectors showing each satellites movement. The distribution of our sample shows a strong correlation around both the LMC and SMC as to be expected. These stronger distributions of our LMC satellites signal the potential locations where our missing satellites are. As seen in Figure 3.2, most of the known and suspected LMC satellites are at a distance ~ 150 kpc from Earth. We can apply this constraint to our distribution to look at which of our satellites are less than or greater than 150 kpc to determine which satellites are potentially detectable with current surveys.

4.1.2 Distance Cutoff of 150 kpc

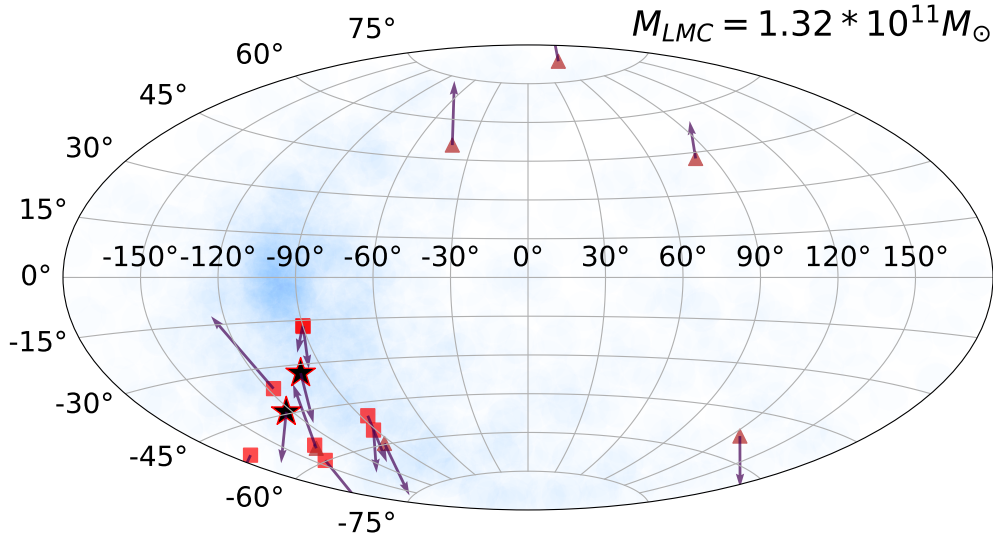


Figure 4.3: We subject our 100 run distribution to project satellites that are $d_{Earth} < 150$ kpc. These are the satellites that are/potentially visible from Earth. All of the references are the same as previously stated.

In Figure 4.3, we show the distribution of our sample satellites that were at a distance less than 150 kpc from Earth. These satellites have the potential of being visible to current surveys like GAIA. The distribution compared to the full distribution of the 100 randomized rotation run concentrates the distribution more near the LMC/SMC and above it in the Galactic plane. We use the same references as in Figure 4.2 and will be the convention for all sequential Aitoff projections. With our list of known/suspected

LMC satellites, this supports why many have found visible satellites with relation to the LMC near the LMC/SMC while only a few suspected satellite are found outside of the near vicinity of the LMC/SMC. The distribution of potentially visible satellites in the Galactic plane is problematic due to the Milky Way disk interfering with our ability to observe fainter objects in this area. There is a lighter distribution of satellites in the southern hemisphere near the southern Galactic pole. Applying our 150 kpc constraint suggests most of the visible satellites current surveys could detect are near the LMC/SMC system or just above it in the Galactic plane, which as we state just a moment ago, is problematic for finding these UFDs of the LMC.

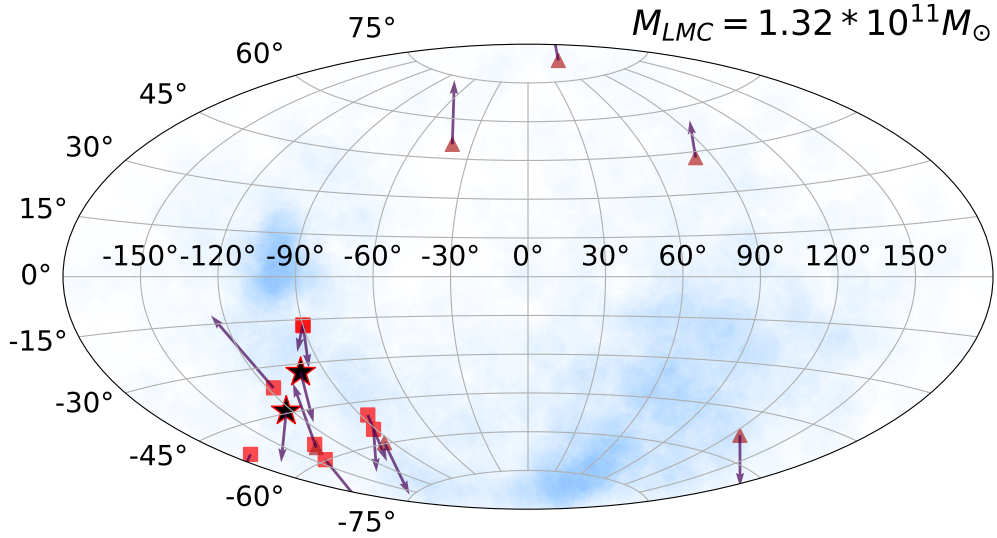


Figure 4.4: We subject our 100 run distribution to project satellites that are $d_{Earth} > 150$ kpc. These are the satellites that are too far from Earth, making their detection improbable to impossible with current surveys like GAIA. All of the references are the same as previously stated. We see satellites are distributed mostly near the Magellanic Stream.

In Figure 4.4, we show the distribution of our sample satellites that were at a distance greater than 150 kpc from Earth. These satellites are potentially at distances too far out to be detected with current surveys. Future surveys may have the ability to detect the more distant dwarf satellites. The distribution compared to the full distribution of the 100 randomized run concentrates the distribution more near the southern Galactic pole in the Magellanic Stream with a slight concentration above the LMC/SMC on the

Galactic plane. We find the distribution of satellites around the LMC/SMC is far less than in Figure 4.3. The distribution of satellites in the Galactic plane are problematic for detection based on the reasons stated previously. There is a higher concentration of satellites near the southern Galactic pole in the Magellanic Stream, suggesting this would be the best place to look to find satellites that originated with the LMC. We need to analyze how many of these satellites are past our 150 kpc distance cutoff. Next, we will look at the Galactocentric distances of our LMC satellites from our model and analyze what percentage of them are past our distance cutoff.

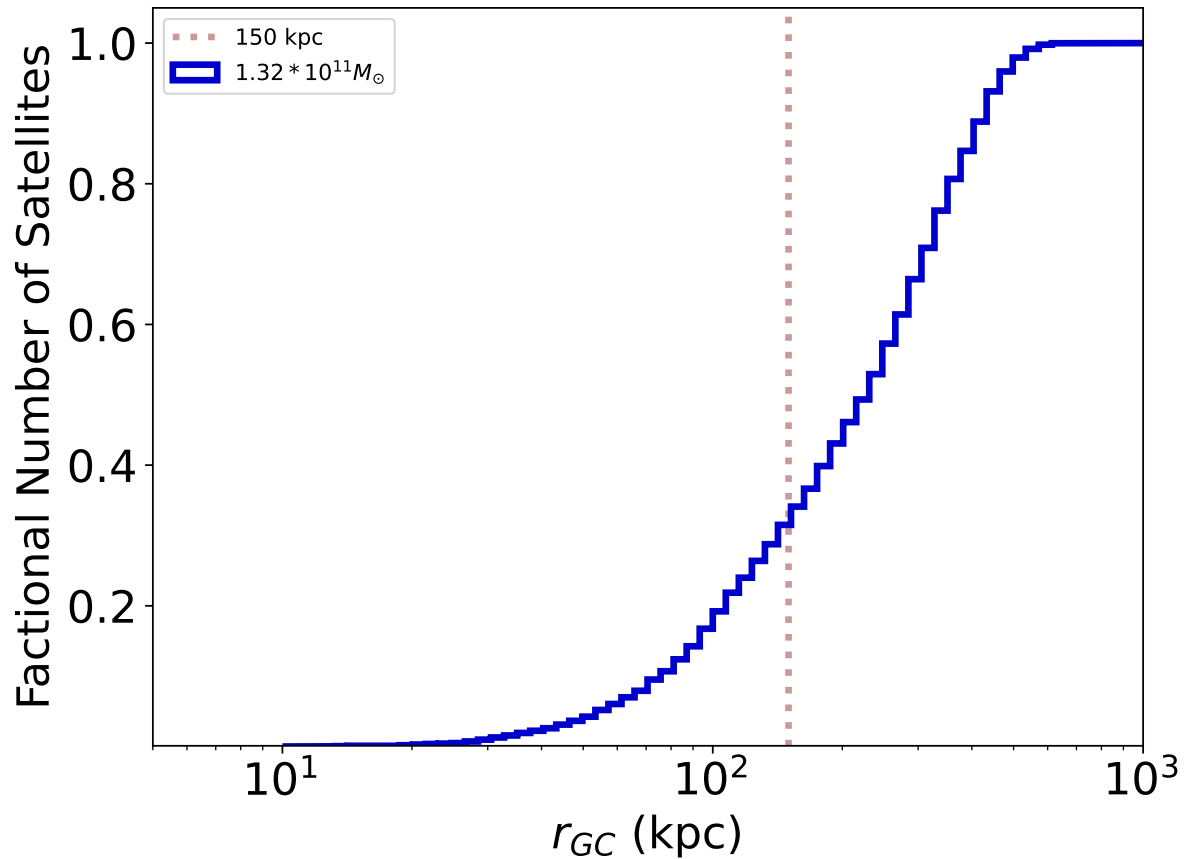


Figure 4.5: From our 100 run sample, we use a normalized cumulative histogram of the distribution with Galactocentric distance from the Milky Way on the x-axis in log and the fractional number of satellites on the y-axis as a cumulative relation of the number of satellites. A vertical dotted line is placed at 150 kpc to show the number of satellites that are within 150 kpc of Earth. We find that a significant portion of the satellites are out past the 150 kpc cutoff.

In Figure 4.5, we show the fractional number of satellites corresponding to their Galactocentric distances from the Milky Way. A dotted red line is placed at 150 kpc, indicating the distance from Earth where satellites are too far out to be detected by current surveys. For our fiducial LMC, we see that there are less than 50% of the satellites are within 150 kpc. The range of satellites based on our fiducial LMC model appears to be between 30% and 40% that would be detectable from current surveys like GAIA and Dark Energy Survey (DES). The two places in Figure 4.3 that have larger distributions are around the LMC/SMC and above it in the Galactic plane. This is problematic for observing satellites as we have previously stated. Greater than 50% of our sample satellites lie beyond the 150 kpc distance cutoff. These satellites are too far out for us to detect and thus why we haven't found them yet. However, based on the distributions in Figure 4.4, we have a prediction of where these satellites could potentially be. Next, we are going to repeat this process for four other LMC masses to compare our results to our fiducial model provided in Table 2.1.

4.2 LMC Mass Dependence

Thanks to the work of Ahvazi et al. (2023), we have access to multiple LMC masses. We can see if there is any correlation between LMC mass and satellite distribution. We will follow the same convention as we did projecting the 100 randomized rotation fiducial model and apply it to the four LMC masses. Of the four additional LMC masses, two of the masses are less than our fiducial ($0.52 \times 10^{11} M_{\odot}$ and $0.91 \times 10^{11} M_{\odot}$) while two of the masses are greater than our fiducial ($2.20 \times 10^{11} M_{\odot}$, and $3.27 \times 10^{11} M_{\odot}$) as

referenced in Table 2.1. Our goal is to see if there is any correlation between the mass of the LMC, it's overall distribution, and the number of satellites at the 150 kpc constraint placed on the fiducial model.

4.2.1 100 Run Mass Dependent LMCs

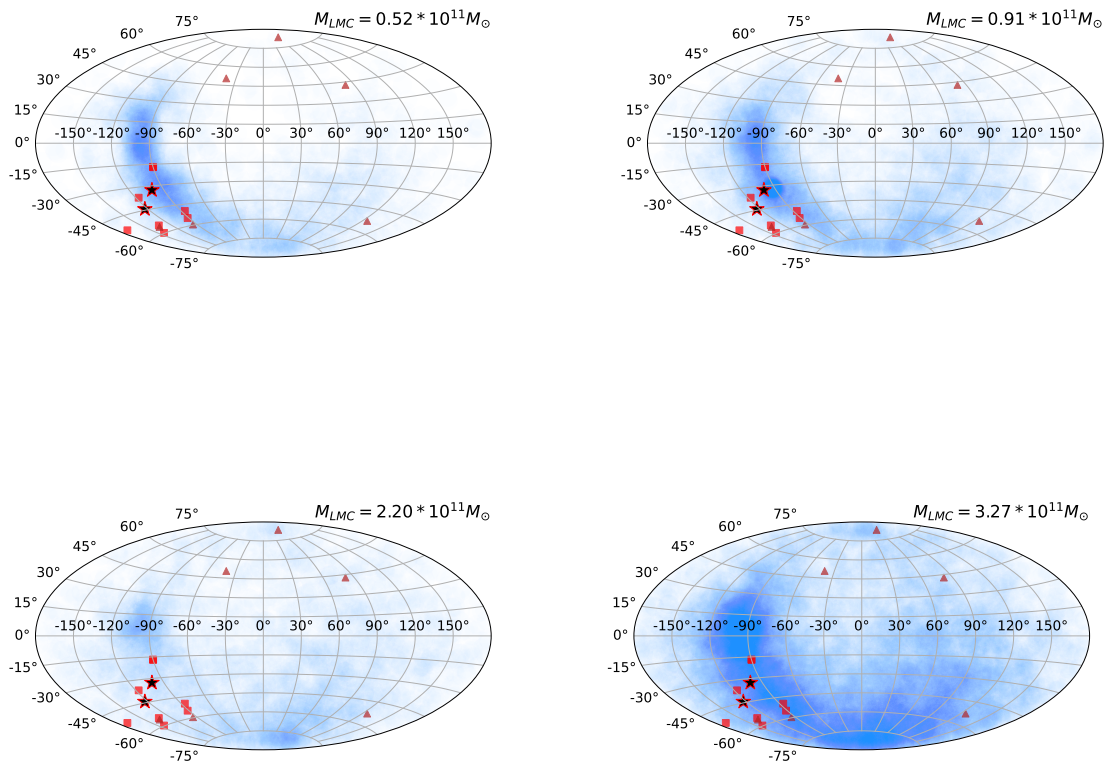


Figure 4.6: The process for Figure 4.2 is repeated for our four LMC masses (from least massive to most: $0.52 \times 10^{11} M_{\odot}$ (top left), $0.91 \times 10^{11} M_{\odot}$ (top right), $2.20 \times 10^{11} M_{\odot}$ (bottom left), and $3.27 \times 10^{11} M_{\odot}$ (bottom right)) All references are present as in previous projections. Although mass affects the scatter on each Aitoff projection, we can see they all have similar distributions to our fiducial model where satellites concentrate around the LMC/SMC, above the LMC/SMC in the Galactic plane, and in the Magellanic Stream.

In Figure 4.6, we compare our fiducial LMC mass ($M = 1.32 \times 10^{11} M_{\odot}$) to our four LMC masses ($0.52 \times 10^{11} M_{\odot}$ (top left), $0.91 \times 10^{11} M_{\odot}$ (top right), $2.20 \times 10^{11} M_{\odot}$ (bottom left), and $3.27 \times 10^{11} M_{\odot}$ (bottom right)). Our Aitoff projections show a consistency of the distribution of satellites for all of our LMC models regardless of mass. There are similar places of distribution for all of our models around the LMC/SMC, above the LMC/SMC in the Galactic plane, and in the Magellanic Stream. Our most massive LMC model has the widest scatter and distribution, however, satellites concentrate across a larger area in the same spots as the other models. Next, we will apply our 150 kpc constraint to our four LMC masses.

4.2.2 Distance Cutoff of 150 kpc for Mass Dependent LMCs

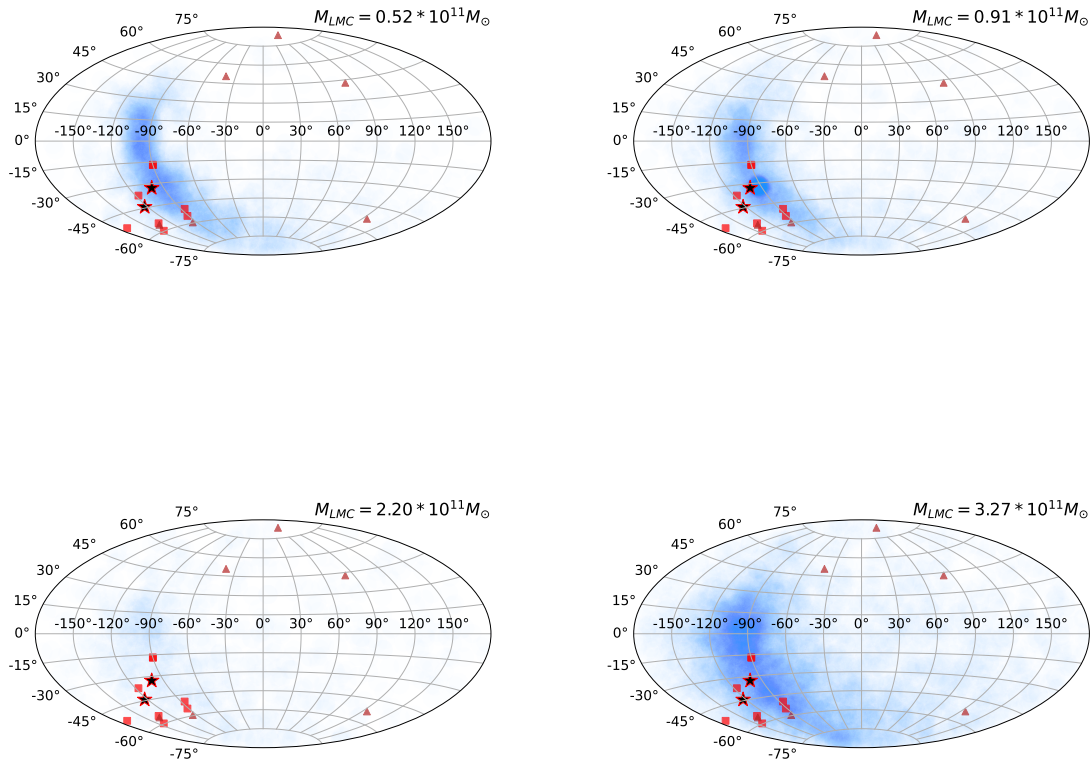


Figure 4.7: We repeat the same process used in Figure 4.3 for our four LMC masses that are < 150 kpc from Earth. The distribution of satellites are around the LMC/SMC and above the LMC/SMC in the Galactic plane, similar to what we see in Fig 4.3. There is not much distribution of satellites in the Magellanic Stream.

In Figure 4.7, we constrain our various LMC masses used in Figure 4.3 to show the satellite distribution of distances < 150 kpc from Earth. Our distribution for our four various massed LMC's follow a similar pattern to that of the fiducial model. We see a higher distribution of satellites are found around the LMC/SMC and above the LMC/SMC in the Galactic plane. The distribution of LMC satellites near the southern Galactic pole is much lower. All these similarities are aligned with what we saw in our fiducial

model, suggesting the potentially more visible satellites are likely to be found around the LMC/SMC or above the LMC/SMC in the Galactic plane, regardless of the mass of our LMC.

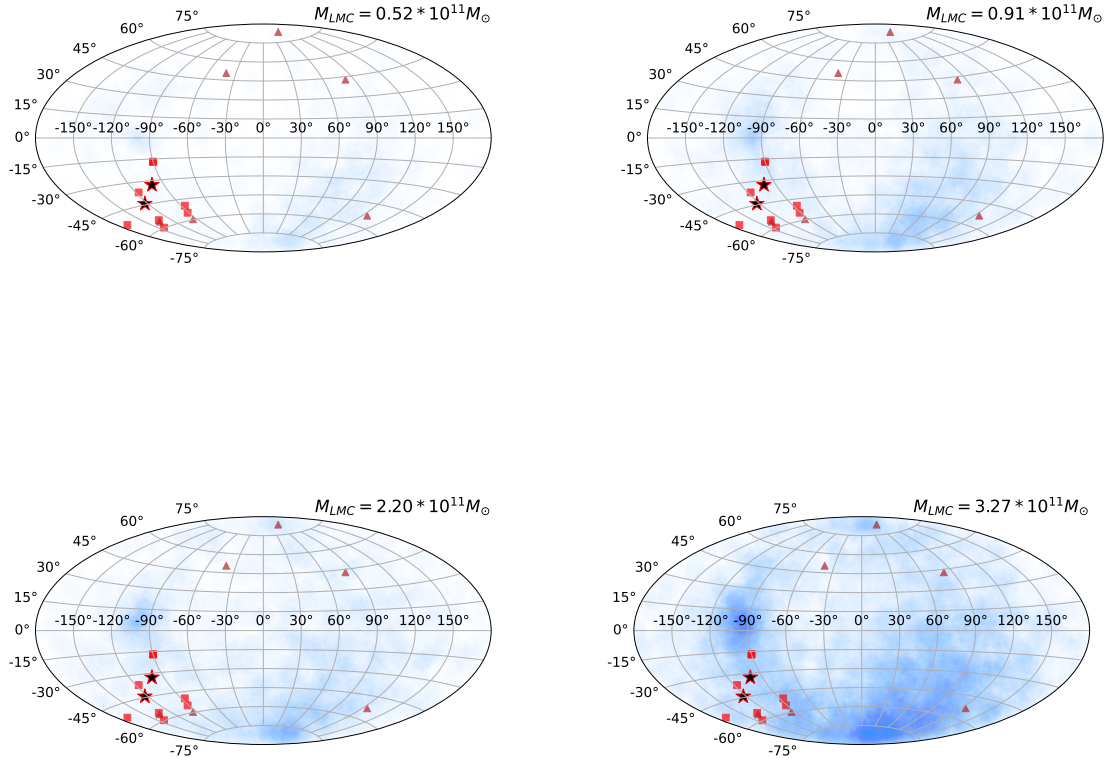


Figure 4.8: We repeat the same process used in Figure 4.4 for our four LMC masses with satellites > 150 kpc from Earth. The distribution of LMC satellites follows a similar pattern to Fig 4.4 for all our models near the southern Galactic pole in the Magellanic Stream. The distribution of satellites around the LMC/SMC and above the LMC/SMC in the Galactic plane is less in our four projections. These results align with what we were seeing in our fiducial LMC model.

In Figure 4.8, we constrain our various LMC masses as we did in Figure 4.4 to LMC satellites > 150 kpc away from Earth. Similar to above and our fiducial LMC model, we find a much lower distribution of satellites around the LMC/SMC and above

the LMC/SMC in the Galactic plane. A greater distribution of satellites is found near the southern Galactic pole in the Magellanic Stream. This would suggest our missing satellites that we cannot see would be located near this location, aligning with what we found in our fiducial model. Our findings suggest LMC mass does not greatly effect the overall results, but suggests that the missing LMC satellites are above the LMC/SMC in the Galactic plane or near the southern Galactic pole. Next, we can look at the fractional satellite distribution relative to their Galactocentric distance to see if there is any correlation between mass and number of satellites that are potentially visible.

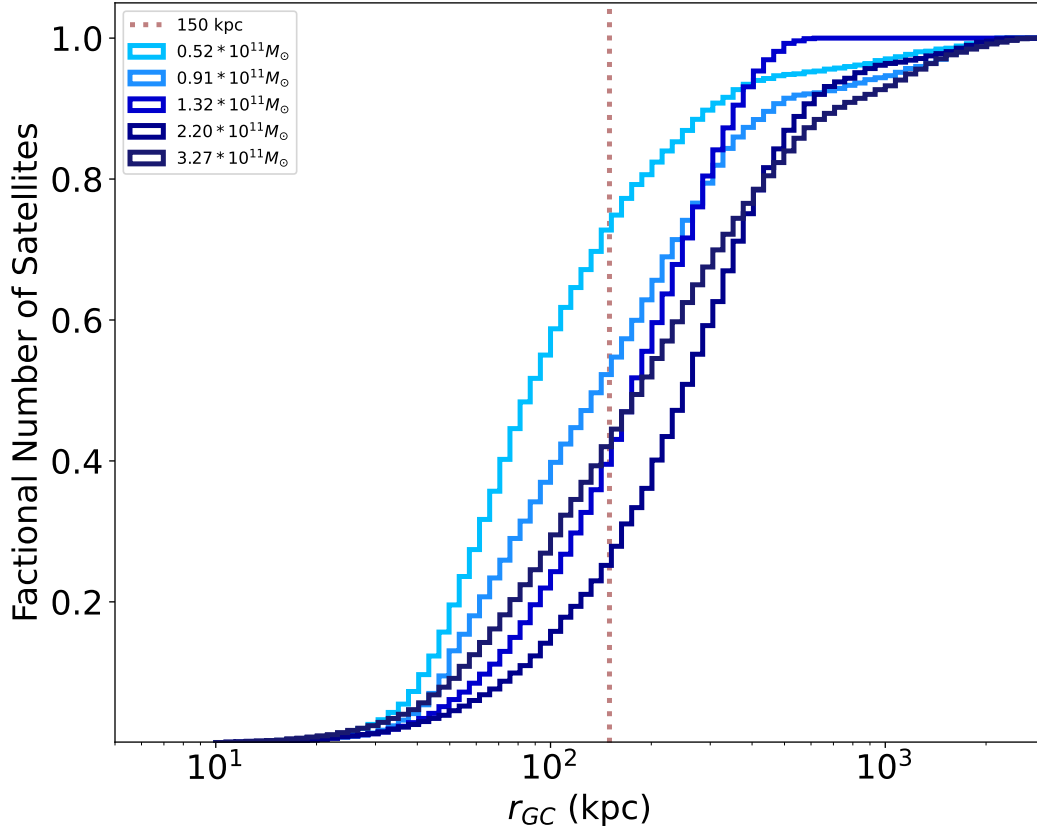


Figure 4.9: We use a normalized cumulative histogram similar to that in Figure 4.5 for all of our LMC model masses. A vertical dotted line is placed at 150 kpc to show the number of satellites that are within 150 kpc of Earth. We find there is a correlation between the fraction of potentially visible satellites in relation to an LMC’s mass. The more massive an LMC is, the less potentially visible satellites there are that can be detected by current surveys.

In Figure 4.9, we show the fractional number of satellites corresponding to their Galactocentric distance from the Milky Way. Our least massive LMC is represented in a light blue, with more massive LMCs represented by darker shades of blue than the one before it. Our fiducial LMC mass uses the same blue as in Figure 4.5. A dotted red line is placed at 150 kpc to show the fractional number of satellites that are less than 150 kpc and greater than 150 kpc. There is a direct correlation to the LMC’s mass and the fractional number of satellites within the 150 kpc from Earth. Our least massive LMC (light blue)

shows $\sim 70\%$ of satellites should be potentially visible versus our most massive LMC (dark blue) shows $\sim 30\%$ of satellites should be potentially visible. Although the mass of the LMC does not effect the overall distribution of satellites, it does have an effect on the fractional number of satellites that would be potentially visible from Earth with current surveys.

Chapter 5

Conclusion

5.1 Conclusion

In this chapter, we summarize the results and conclusions presented in this thesis. We presented a question that has been asked since Bovill & Ricotti (2011); the LMC should have more satellites around it but where are they?

To answer this question, we had to build a model of the LMC with satellites in orbit around it on first infall into the Milky Way. Our model is built using the python package `Galpy` to build our Milky Way and LMC potentials, create a moving potential with dynamical friction, place LMC satellites as test particles orbiting the LMC, and move our LMC with satellites orbiting it into the Milky Way to find out where the satellites are positioned. By introducing randomized rotations to our satellites as they go through first infall, we can build statistics to further support our findings.

To better understand our findings, we use the findings of Erkal & Belokurov (2020), Patel et al. (2020), Battaglia et al. (2022), Vasiliev (2023), and other who have done work to identify known and potential LMC satellites. Using their findings, we can compare their place around the LMC and distance from Earth to estimate how far out these satellites are. This cutoff at 150 kpc (from Earth) allows us to make the assumption that any satellites past this cutoff are too far out for us to observe. Our model is repeated for various LMC masses thanks to the findings of (Ahvazi et al. 2023). This allows us to probe further about what lower mass and higher mass LMC's do to the distribution of it's satellites upon first infall.

Our conclusions are as follows.

- Our model is able to reproduce the Magellanic Cloud system from the distribution of the LMC's satellite orbits.
- With our applied constraint of 150 kpc, we showed the distribution of satellites that had $r_{GC} < 150$ kpc were around the LMC/SMC system and above the LMC/SMC in the Galactic plane. The satellites that were $r_{GC} > 150$ kpc had a concentrated distribution near the southern Galactic pole in the Magellanic Stream.
- The distribution of the fractional number of satellites versus distance for our fiducial model shows between 30% to 40% of the LMC satellites are within the 150 kpc distance cutoff. Over 50% of the missing satellites are found beyond the distance cutoff.
- Looking at our various LMC mass models, we found that mass of the LMC does not affect the distribution of satellites. However, there is a direct correlation between the fractional number of satellites within 150 kpc cutoff and LMC mass. Increasing LMC mass leads to less fractional satellites found within 150 kpc.
- Some of the LMC satellites are shown to reside in the Galactic plane, making them problematic for finding. However, our models show that there is a distribution of LMC satellites near the southern Galactic pole. If further research is done trying to find the LMC's missing satellites, the results of this thesis point to the Magellanic Stream near the southern Galactic pole as a place to look.

This work shows the ability to get a distribution of satellites for varying LMC masses.

Our models are able to replicate a moving LMC system with orbiting satellites interacting

with the Milky Way and show the distribution of the satellite's positions after the model runs. Further, our models can show the distribution of satellites in the system and point to where a search for the missing satellites could be.

5.2 Looking to the Future

5.2.1 N-body Simulations for LMC satellites

In Chapter 2, we discussed our process for setting up our model. The use of test particles helped to simplify the model. Future work would be to refine our LMC potential model to include an LMC disk similar to the works of Patel et al. (2020). Further, we can find the kinematics of the known/suspected LMC dwarfs to set up an N-body simulation to run in our model and build statistical data for those satellite's orbits. Exploration into the binding energy of our satellites after first infall was looked at in this thesis. However, the results were peculiar and require further review into what is really happening. Additionally, the ability to orbit satellites around the Milky potential and simulate satellite capture by the LMC could be explored.

5.2.2 Curiosities Surrounding M33

The results of our research proved we can replicate galaxy's moving through one and another with satellite's orbiting them during their interactions. We posed the question at the beginning of this thesis asking where the missing LMC satellites were. A more curious case surrounds M33 which has far fewer known satellites in orbit around it than

it should. What happened to all these satellites and why do we see so few of them. Using the modeling we did in this work, we know we could run a model for M33 and potentially answer that question.

Bibliography

2010, Chemical Abundances in the Universe: Connecting First Stars to Planets, Vol. 265

Aghanim, N., Akrami, Y., Ashdown, M., Aumont, J., Baccigalupi, C., Ballardini, M., Banday, A. J., Barreiro, R. B., Bartolo, N., Basak, S., Battye, R., Benabed, K., Bernard, J.-P., Bersanelli, M., Bielewicz, P., Bock, J. J., Bond, J. R., Borrill, J., Bouchet, F. R., Boulanger, F., Bucher, M., Burigana, C., Butler, R. C., Calabrese, E., Cardoso, J.-F., Carron, J., Challinor, A., Chiang, H. C., Chluba, J., Colombo, L. P. L., Combet, C., Contreras, D., Crill, B. P., Cuttaia, F., de Bernardis, P., de Zotti, G., Delabrouille, J., Delouis, J.-M., Di Valentino, E., Diego, J. M., Doré, O., Douspis, M., Ducout, A., Dupac, X., Dusini, S., Efstathiou, G., Elsner, F., Enßlin, T. A., Eriksen, H. K., Fantaye, Y., Farhang, M., Fergusson, J., Fernandez-Cobos, R., Finelli, F., Forastieri, F., Frailis, M., Fraisse, A. A., Franceschi, E., Frolov, A., Galeotta, S., Galli, S., Ganga, K., Génova-Santos, R. T., Gerbino, M., Ghosh, T., González-Nuevo, J., Górski, K. M., Gratton, S., Gruppuso, A., Gudmundsson, J. E., Hamann, J., Handley, W., Hansen, F. K., Herranz, D., Hildebrandt, S. R., Hivon, E., Huang, Z., Jaffe, A. H., Jones, W. C., Karakci, A., Kihänen, E., Keskitalo, R., Kiiveri, K., Kim, J., Kisner, T. S., Knox, L., Krachmalnicoff, N., Kunz, M., Kurki-Suonio, H., Lagache, G., Lamarre, J.-M., Lasenby, A., Lattanzi, M., Lawrence, C. R., Le Jeune, M., Lemos, P., Lesgourgues, J., Levrier, F., Lewis, A., Liguori, M., Lilje, P. B., Lilley, M., Lindholm, V., López-Caniego, M., Lubin, P. M., Ma, Y.-Z., Macías-Pérez, J. F., Maggio, G., Maino, D., Mandolesi, N., Mangilli, A., Marcos-Caballero, A., Maris, M., Martin, P. G., Martinelli, M., Martínez-González, E., Matarrese, S., Mauri, N., McEwen, J. D., Meinhold, P. R., Melchiorri, A., Mennella, A., Migliaccio, M., Millea, M., Mitra, S., Miville-Deschênes, M.-A., Molinari, D., Montier, L., Morgante, G., Moss, A., Natoli, P., Nørgaard-Nielsen, H. U., Pagano, L., Paoletti, D., Partridge, B., Patanchon, G., Peiris, H. V., Perrotta, F., Pettorino, V., Piacentini, F., Polastri, L., Polenta, G., Puget, J.-L., Rachen, J. P., Reinecke, M., Remazeilles, M., Renzi, A., Rocha, G., Rosset, C., Roudier, G., Rubiño-Martín, J. A., Ruiz-Granados, B., Salvati, L., Sandri, M., Savelainen, M., Scott, D., Shellard, E. P. S., Sirignano, C., Sirri, G., Spencer, L. D., Sunyaev, R., Suur-Uski, A.-S., Tauber, J. A., Tavagnacco, D., Tenti, M., Toffolatti, L., Tomasi, M., Trombetti, T., Valenziano, L., Valiviita, J., Van Tent, B., Vibert, L., Vielva, P., Villa, F., Vittorio, N., Wandelt, B. D., Wehus, I. K., White, M., White, S. D. M., Zacchei, A., & Zonca, A. 2020, *Astronomy and Astrophysics*, 641, A6

- Ahvazi, N., Benson, A., Sales, L. V., Nadler, E. O., Weerasooriya, S., Du, X., & Bovill, M. S. 2023, arXiv e-prints, arXiv:2308.13599
- Alexander, R. K., Vincenzo, F., Ji, A. P., Richstein, H., Jordan, C. J., & Gibson, B. K. 2023, *Monthly Notices of the Royal Astronomy Society*, 522, 5415
- Barger, K., Frazer, E. M., & Fox, A. J. 2019, in *American Astronomical Society Meeting Abstracts*, Vol. 233, *American Astronomical Society Meeting Abstracts #233*, 256.03
- Battaglia, G., Taibi, S., Thomas, G. F., & Fritz, T. K. 2022, *Astronomy and Astrophysics*, 657, A54
- Benson, A. 2011, *Galacticus: A Semi-Analytic Model of Galaxy Formation*, *Astrophysics Source Code Library*, record ascl:1108.004
- Besla, G., Kallivayalil, N., Hernquist, L., Robertson, B., Cox, T. J., van der Marel, R. P., & Alcock, C. 2007, *The Astrophysical Journal*, 668, 949
- Bovill, M. S. & Ricotti, M. 2009, *The Astrophysical Journal*, 693, 1859
- . 2011, *The Astrophysical Journal*, 741, 17
- Bovy, J. 2015, *Astrophysical Journal Supplement*, 216, 29
- Bovy, J. & Rix, H.-W. 2013, *The Astrophysical Journal*, 779, 115
- Deason, A. J., Wetzel, A. R., Garrison-Kimmel, S., & Belokurov, V. 2015, *Monthly Notices of the Royal Astronomy Society*, 453, 3568
- Erkal, D. 2019, in *A Synoptic View of the Magellanic Clouds: VMC, Gaia and Beyond*, 33
- Erkal, D., Belokurov, V., Laporte, C. F. P., Koposov, S. E., Li, T. S., Grillmair, C. J., Kallivayalil, N., Price-Whelan, A. M., Evans, N. W., Hawkins, K., Hendel, D., Mateu, C., Navarro, J. F., del Pino, A., Slater, C. T., & Sohn, S. T. 2019, *Monthly Notices of the Royal Astronomical Society*, 487, 2685–2700
- Erkal, D. & Belokurov, V. A. 2020, *Monthly Notices of the Royal Astronomy Society*, 495, 2554
- Evans, N. W. & Wilkinson, M. I. 2000, *Monthly Notices of the Royal Astronomy Society*, 316, 929
- Gaia Collaboration, Brown, A. G. A., Vallenari, A., Prusti, T., de Bruijne, J. H. J., Babusiaux, C., Bailer-Jones, C. A. L., Biermann, M., Evans, D. W., Eyer, L., Jansen, F., Jordi, C., Klioner, S. A., Lammers, U., Lindegren, L., Luri, X., Mignard, F., Panem, C., Pourbaix, D., Randich, S., Sartoretti, P., Siddiqui, H. I., Soubiran, C., van Leeuwen, F., Walton, N. A., Arenou, F., Bastian, U., Cropper, M., Drimmel, R., Katz, D., Lattanzi, M. G., Bakker, J., Cacciari, C., Castañeda, J., Chaoul, L., Cheek, N., De Angeli, F., Fabricius, C., Guerra, R., Holl, B., Masana, E., Messineo, R., Mowlavi,

N., Nienartowicz, K., Panuzzo, P., Portell, J., Riello, M., Seabroke, G. M., Tanga, P., Thévenin, F., Gracia-Abril, G., Comoretto, G., Garcia-Reinaldos, M., Teyssier, D., Altmann, M., Andrae, R., Audard, M., Bellas-Velidis, I., Benson, K., Berthier, J., Blomme, R., Burgess, P., Busso, G., Carry, B., Cellino, A., Clementini, G., Clotet, M., Creevey, O., Davidson, M., De Ridder, J., Delchambre, L., Dell'Oro, A., Ducourant, C., Fernández-Hernández, J., Fouesneau, M., Frémat, Y., Galluccio, L., García-Torres, M., González-Núñez, J., González-Vidal, J. J., Gosset, E., Guy, L. P., Halbwachs, J. L., Hambly, N. C., Harrison, D. L., Hernández, J., Hestroffer, D., Hodgkin, S. T., Hutton, A., Jasniewicz, G., Jean-Antoine-Piccolo, A., Jordan, S., Korn, A. J., Krone-Martins, A., Lanzafame, A. C., Lebzelter, T., Löffler, W., Manteiga, M., Marrese, P. M., Martín-Fleitas, J. M., Moitinho, A., Mora, A., Muinonen, K., Osinde, J., Pancino, E., Pauwels, T., Petit, J. M., Recio-Blanco, A., Richards, P. J., Rimoldini, L., Robin, A. C., Sarro, L. M., Siopis, C., Smith, M., Sozzetti, A., Süveges, M., Torra, J., van Reeven, W., Abbas, U., Abreu Aramburu, A., Accart, S., Aerts, C., Altavilla, G., Álvarez, M. A., Alvarez, R., Alves, J., Anderson, R. I., Andrei, A. H., Anglada Varela, E., Antiche, E., Antoja, T., Arcay, B., Astraatmadja, T. L., Bach, N., Baker, S. G., Balaguer-Núñez, L., Balm, P., Barache, C., Barata, C., Barbato, D., Barblan, F., Barklem, P. S., Barrado, D., Barros, M., Barstow, M. A., Bartholomé Muñoz, S., Bassilana, J. L., Becciani, U., Bellazzini, M., Berihuete, A., Bertone, S., Bianchi, L., Bienaymé, O., Blanco-Cuaresma, S., Boch, T., Boeche, C., Bombrun, A., Borrachero, R., Bossini, D., Bouquillon, S., Bourda, G., Bragaglia, A., Bramante, L., Breddels, M. A., Bressan, A., Brouillet, N., Brüsemeister, T., Brugaletta, E., Bucciarelli, B., Burlacu, A., Busonero, D., Butkevich, A. G., Buzzzi, R., Caffau, E., Cancelliere, R., Cannizzaro, G., Cantat-Gaudin, T., Carballo, R., Carlucci, T., Carrasco, J. M., Casamiquela, L., Castellani, M., Castro-Ginard, A., Charlot, P., Chemin, L., Chiavassa, A., Cocozza, G., Costigan, G., Cowell, S., Crifo, F., Crosta, M., Crowley, C., Cuypers, J., Dafonte, C., Damerdj, Y., Dapergolas, A., David, P., David, M., de Laverny, P., De Luise, F., De March, R., de Martino, D., de Souza, R., de Torres, A., Debosscher, J., del Pozo, E., Delbo, M., Delgado, A., Delgado, H. E., Di Matteo, P., Diakite, S., Diener, C., Distefano, E., Dolding, C., Drazinos, P., Durán, J., Edvardsson, B., Enke, H., Eriksson, K., Esquej, P., Eynard Bontemps, G., Fabre, C., Fabrizio, M., Faigler, S., Falcão, A. J., Farràs Casas, M., Federici, L., Fedorets, G., Fernique, P., Figueras, F., Filippi, F., Findeisen, K., Fonti, A., Fraile, E., Fraser, M., Frézouls, B., Gai, M., Galleti, S., Garabato, D., García-Sedano, F., Garofalo, A., Garralda, N., Gavel, A., Gavras, P., Gerssen, J., Geyer, R., Giacobbe, P., Gilmore, G., Girona, S., Giuffrida, G., Glass, F., Gomes, M., Granvik, M., Gueguen, A., Guerrier, A., Guiraud, J., Gutiérrez-Sánchez, R., Haigron, R., Hatzidimitriou, D., Hauser, M., Haywood, M., Heiter, U., Helmi, A., Heu, J., Hilger, T., Hobbs, D., Hofmann, W., Holland, G., Huckle, H. E., Hypki, A., Icardi, V., Janßen, K., Jevardat de Fombelle, G., Jonker, P. G., Juhász, Á. L., Julbe, F., Karampelas, A., Kewley, A., Klar, J., Kochoska, A., Kohley, R., Kolenberg, K., Kontizas, M., Kontizas, E., Kopusov, S. E., Kordopatis, G., Kostrzewa-Rutkowska, Z., Koubsky, P., Lambert, S., Lanza, A. F., Lasne, Y., Lavigne, J. B., Le Fustec, Y., Le Poncin-Lafitte, C., Lebreton, Y., Leccia, S., Leclerc, N., Lecoœur-Taïbi, I., Lenhardt, H., Leroux, F., Liao, S., Licata, E., Lindstrøm, H. E. P., Lister, T. A., Livanou, E., Lobel, A., López, M., Managau, S., Mann, R. G., Mantelet, G., Marchal,

- O., Marchant, J. M., Marconi, M., Marinoni, S., Marschalkó, G., Marshall, D. J., Martino, M., Marton, G., Mary, N., Massari, D., Matijević, G., Mazeh, T., McMillan, P. J., Messina, S., Michalik, D., Millar, N. R., Molina, D., Molinaro, R., Molnár, L., Montegriffo, P., Mor, R., Morbidelli, R., Morel, T., Morris, D., Mulone, A. F., Muraveva, T., Musella, I., Nelemans, G., Nicastrò, L., Noval, L., O'Mullane, W., Ordénovic, C., Ordóñez-Blanco, D., Osborne, P., Pagani, C., Pagano, I., Paillet, F., Palacin, H., Palaversa, L., Panahi, A., Pawlak, M., Piersimoni, A. M., Pineau, F. X., Plachy, E., Plum, G., Poggio, E., Poujoulet, E., Prša, A., Pulone, L., Racero, E., Ragaini, S., Rambaux, N., Ramos-Lerate, M., Regibo, S., Reylé, C., Rielet, F., Ripepi, V., Riva, A., Rivard, A., Rixon, G., Roegiers, T., Roelens, M., Romero-Gómez, M., Rowell, N., Royer, F., Ruiz-Dern, L., Sadowski, G., Sagristà Sellés, T., Sahlmann, J., Salgado, J., Salguero, E., Sanna, N., Santana-Ros, T., Sarasso, M., Saviotto, H., Schultheis, M., Sciacca, E., Segol, M., Segovia, J. C., Ségransan, D., Shih, I. C., Siltala, L., Silva, A. F., Smart, R. L., Smith, K. W., Solano, E., Solitro, F., Sordo, R., Soria Nieto, S., Souchay, J., Spagna, A., Spoto, F., Stampa, U., Steele, I. A., Steidelmüller, H., Stephenson, C. A., Stoev, H., Suess, F. F., Surdej, J., Szabados, L., Szegedi-Elek, E., Tapiador, D., Taris, F., Tauran, G., Taylor, M. B., Teixeira, R., Terrett, D., Teyssandier, P., Thuillot, W., Titarenko, A., Torra Clotet, F., Turon, C., Ulla, A., Utrilla, E., Uzzi, S., Vaillant, M., Valentini, G., Valette, V., van Elteren, A., Van Hemelryck, E., van Leeuwen, M., Vaschetto, M., Vecchiato, A., Veljanoski, J., Viala, Y., Vicente, D., Vogt, S., von Essen, C., Voss, H., Votruba, V., Voutsinas, S., Walmsley, G., Weiler, M., Wertz, O., Wevers, T., Wyrzykowski, L., Yoldas, A., Žerjal, M., Ziaepour, H., Zorec, J., Zschocke, S., Zucker, S., Zurbach, C., & Zwitter, T. 2018, *Astronomy and Astrophysics*, 616, A1
- Hoekstra, H., Bartelmann, M., Dahle, H., Israel, H., Limousin, M., & Meneghetti, M. 2013, *Space Science Reviews*, 177, 75–118
- Kallivayalil, N., Sales, L. V., Zivick, P., Fritz, T. K., Del Pino, A., Sohn, S. T., Besla, G., van der Marel, R. P., Navarro, J. F., & Sacchi, E. 2018, *The Astrophysical Journal*, 867, 19
- Kleyna, J. T., Wilkinson, M. I., Evans, N. W., & Gilmore, G. 2001, *The Astrophysical Journal Letters*, 563, L115
- Knebe, A., Stoppacher, D., Prada, F., Behrens, C., Benson, A., Cora, S. A., Croton, D. J., Padilla, N. D., Ruiz, A. N., Sinha, M., Stevens, A. R. H., Vega-Martínez, C. A., Behroozi, P., Gonzalez-Perez, V., Gottlöber, S., Klypin, A. A., Yepes, G., Enke, H., Libeskind, N. I., Riebe, K., & Steinmetz, M. 2018, *Monthly Notices of the Royal Astronomy Society*, 474, 5206
- Mateo, M., Olszewski, E. W., Vogt, S. S., & Keane, M. J. 1998, *The Astronomical Journal*, 116, 2315
- McConnachie, A. W. 2012, *The Astronomical Journal*, 144, 4

- Pardy, S. A., D'Onghia, E., Navarro, J. F., Grand, R., Gómez, F. A., Marinacci, F., Pakmor, R., Simpson, C., & Springel, V. 2020, *Monthly Notices of the Royal Astronomy Society*, 492, 1543
- Patel, E., Kallivayalil, N., Garavito-Camargo, N., Besla, G., Weisz, D. R., van der Marel, R. P., Boylan-Kolchin, M., Pawlowski, M. S., & Gómez, F. A. 2020, *The Astrophysical Journal*, 893, 121
- Press, W. H. & Schechter, P. 1974, *The Astrophysical Journal*, 187, 425
- Richstein, H., Kallivayalil, N., Simon, J. D., Garling, C. T., Wetzel, A., Warfield, J. T., van der Marel, R. P., Jeon, M., Rose, J. C., Torrey, P., Engelhardt, A. C., Besla, G., Choi, Y., Geha, M., Guhathakurta, P., Kirby, E. N., Patel, E., Sacchi, E., & Sohn, S. T. 2024, arXiv e-prints, arXiv:2402.08731
- Rubin, V. C. & Ford, W. Kent, J. 1970, *The Astrophysical Journal*, 159, 379
- Sacchi, E., Richstein, H., Kallivayalil, N., van der Marel, R., Libralato, M., Zivick, P., Besla, G., Brown, T. M., Choi, Y., Deason, A., Fritz, T., Geha, M., Guhathakurta, P., Jeon, M., Kirby, E., Majewski, S. R., Patel, E., Simon, J. D., Tony Sohn, S., Tollerud, E., & Wetzel, A. 2021, *The Astrophysical Journal Letters*, 920, L19
- Sales, L. V., Navarro, J. F., Kallivayalil, N., & Frenk, C. S. 2017, *Monthly Notices of the Royal Astronomy Society*, 465, 1879
- Somerville, R. S. & Primack, J. R. 1999, *Monthly Notices of the Royal Astronomy Society*, 310, 1087
- Vasiliev, E. 2023, *Galaxies*, 11, 59
- Weerasooriya, S., Bovill, M. S., Benson, A., Musick, A. M., & Ricotti, M. 2023, *The Astrophysical Journal*, 948, 87
- Weerasooriya, S., Bovill, M. S., Taylor, M. A., Benson, A. J., & Leahy, C. 2023, *Devouring The Centaurus A Satellites: Modeling Dwarf Galaxies with Galacticus*
- Wilkinson, M. I., Kleyna, J. T., Gilmore, G. F., Evans, N. W., Koch, A., Grebel, E. K., Wyse, R. F. G., & Harbeck, D. R. 2006, *The Messenger*, 124, 25

VITA

Iver Sneva was born August 30th, 1993 in White Bear Lake, Minnesota. He is the oldest son to Lisa and Frank Sherman. Graduating in 2018 from the University of North Texas, he received his Bachelor of Arts degrees in two entirely separate disciplines of Physics and Music. In August of 2021, he enrolled in graduate studies at Texas Christian University, working towards a Masters of Science in Physics & Astronomy. Since 2021, he has worked for Texas Christian University as a teaching assistant in the Physics & Astronomy department and as a graduate assistant with the Koehler Center.

Personal Background Iver Sneva

White Bear Lake, MN

Son of Lisa and Frank Sherman

Education

Diploma, White Bear Lake Area High Schools,
White Bear Lake, MN, 2011

Bachelor of Arts, Physics, University of North Texas,
Denton, TX, 2018

Bachelor of Arts, Music, University of North Texas,
Denton, TX, 2018

Master of Science, Physics and Astronomy, Texas Christian
University, Fort Worth, TX, 2024

Experience

Graduate Assistantship, Texas Christian University,
Fort Worth, TX, 2022-2024

Teaching Assistantship, Texas Christian University,
Fort Worth, TX, 2021-2022

ABSTRACT

THE LMC SATELLITES, WHERE ARE THEY? A MODEL OF THE LMC'S FIRST INFALL

by Iver B Sneva, Masters, 2024
Department of Physics and Astronomy
Texas Christian University

Research Advisor: Dr. Mia Bovill, Research Scientist University of Maryland

Until recently, we have not been able to observe satellites orbiting the LMC but that all changed with GAIA DR2. Research into dwarf galaxy's found satellites orbiting the Large Magellanic Cloud (LMC). However, the number of satellites around the LMC is still low. We want to find these missing satellites. We set out to build a model of the LMC moving toward first infall with the Milky Way using a semi-analytic model with H_2 cooling to look where the satellites orbiting the LMC end up. Our work aims to reproduce an accurate LMC-MW model and find where these missing LMC satellites have ended up. Our results show that LMC mass does not affect the distribution of satellites in our model, but affects the number of satellites observable with current surveys. Additionally, we find the locations where these missing satellites are.